



Peripheral CD8⁺ T cell characteristics associated with durable responses to immune checkpoint blockade in patients with metastatic melanoma

Benjamin P. Fairfax^{ID 1,2,3}✉, Chelsea A. Taylor^{1,2}, Robert A. Watson^{1,2}, Isar Nassiri^{1,2}, Sara Danielli^{2,3}, Hai Fang^{ID 4}, Elise A. Mahé^{1,2}, Rosalin Cooper^{1,2}, Victoria Woodcock^{ID 2}, Zoe Traill⁵, M. Hussein Al-Mossawi^{ID 6}, Julian C. Knight^{ID 3,4}, Paul Klenerman^{3,7}, Miranda Payne² and Mark R. Middleton^{ID 2,3}

Immune checkpoint blockade (ICB) of PD-1 and CTLA-4 to treat metastatic melanoma (MM) has variable therapeutic benefit. To explore this in peripheral samples, we characterized CD8⁺ T cell gene expression across a cohort of patients with MM receiving anti-PD-1 alone (sICB) or in combination with anti-CTLA-4 (cICB). Whereas CD8⁺ transcriptional responses to sICB and cICB involve a shared gene set, the magnitude of cICB response is over fourfold greater, with preferential induction of mitosis- and interferon-related genes. Early samples from patients with durable clinical benefit demonstrated overexpression of T cell receptor-encoding genes. By mapping T cell receptor clonality, we find that responding patients have more large clones (those occupying >0.5% of repertoire) post-treatment than non-responding patients or controls, and this correlates with effector memory T cell percentage. Single-cell RNA-sequencing of eight post-treatment samples demonstrates that large clones overexpress genes implicated in cytotoxicity and characteristic of effector memory T cells, including CCL4, GNLY and NKG7. The 6-month clinical response to ICB in patients with MM is associated with the large CD8⁺ T cell clone count 21 d after treatment and agnostic to clonal specificity, suggesting that post-ICB peripheral CD8⁺ clonality can provide information regarding long-term treatment response and, potentially, facilitate treatment stratification.

Predictive markers of sensitivity to immune checkpoint blockade (ICB) can be inferred from attributes of the tumor, including mutation burden and infiltrating lymphocytes^{1–5}. However, peripheral markers of on-treatment assessment of efficacy are lacking^{6–8}. Numerous factors independent of the tumor potentially impact the response to ICB^{9–11}. We reasoned that large-scale transcriptomic analysis of peripheral immune subsets might identify conserved features of the response to ICB, including markers predictive of clinical outcome. We analyzed transcript expression in CD8⁺ T cells, which play a key role in the immune response to melanoma¹², across an initial cohort of 55 patients treated with anti-PD-1 alone (sICB; $n=40$) or with anti-CTLA-4 (cICB; $n=15$; Supplementary Table 1). By comparing baseline expression profiles (day 0) with those

post-treatment (day 21), we identified 707 and 5,885 transcripts (false discovery rate (FDR) <0.05) modulated by sICB and cICB, respectively (Fig. 1a,b and Supplementary Table 2). Comparing sICB response to cICB response revealed 4,601 transcripts (FDR <0.05) differentially regulated by cICB versus sICB (Fig. 1c and Supplementary Table 2), with both treatments almost invariably eliciting the same directional effect and hence regulating a shared gene set, but with a marked difference in effect size (Fig. 1d). Most transcriptional changes resolved by the fourth cycle of treatment post-sICB, whereas 877 transcripts remained differentially expressed versus baseline post-cICB (Extended Data Fig. 1a), illustrating that cICB leads to a more sustained effect on transcription. Gene set enrichment analysis identified 25 pathways (FDR <0.01) either preferentially upregulated by cICB, such as genes involved in mitotic spindle formation and G2M checkpoint, or downregulated, including tumor-necrosis factor signaling via NFκB (Fig. 1e,f and Extended Data Fig. 1b), reflecting relatively enhanced cellular proliferation and suppressed inflammation.

The use of RNA-sequencing (RNA-seq) and the number of paired samples across the cohort significantly advance previous transcriptomic descriptions of ICB response in humans, which have indicated few associations robust to multiple-testing correction^{12–14}. To further dissect individual variation in ICB response, we performed weighted-gene centric network analysis to identify modules of co-expressed ICB-regulated transcripts^{15,16}. This approach resolved nine independently correlated modules (modules M1–M9, Supplementary Table 3) with specific hub genes, of which seven were highly enriched for genes from 59 distinct pathways annotated using Gene Ontology Biological Processes (GOBP, Extended Data Fig. 2). Notably, for several modules, the average expression significantly differed between pre-treated patients and healthy controls, between treatment types and across treatment timepoints (Extended Data Fig. 3). Between baseline patient and control samples this difference was most significant in modules M3 and M4, indicating suppression of signal transduction and higher cell division in patient samples, respectively, consistent with induction of cell-cycle genes in exhausted T cells in patients with MM¹². ICB robustly upregulated several modules with larger effects in cICB, the foremost being

¹MRC-Weatherall Institute of Molecular Medicine, University of Oxford, Oxford, UK. ²Department of Oncology, University of Oxford & Oxford Cancer Centre, Churchill Hospital, Oxford University Hospitals NHS Foundation Trust, Oxford, UK. ³NIHR Oxford Biomedical Research Centre, Oxford University Hospitals NHS Foundation Trust, Oxford, UK. ⁴Wellcome Centre for Human Genetics, Nuffield Department of Medicine, University of Oxford, Oxford, UK. ⁵Department of Radiology, Churchill Hospital, Oxford University Hospitals NHS Foundation Trust, Oxford, UK. ⁶Botnar Research Centre, NDORMS, University of Oxford, Oxford, UK. ⁷Translational Gastroenterology Unit, John Radcliffe Hospital, Oxford, UK. ✉e-mail: benjamin.fairfax@oncology.ox.ac.uk

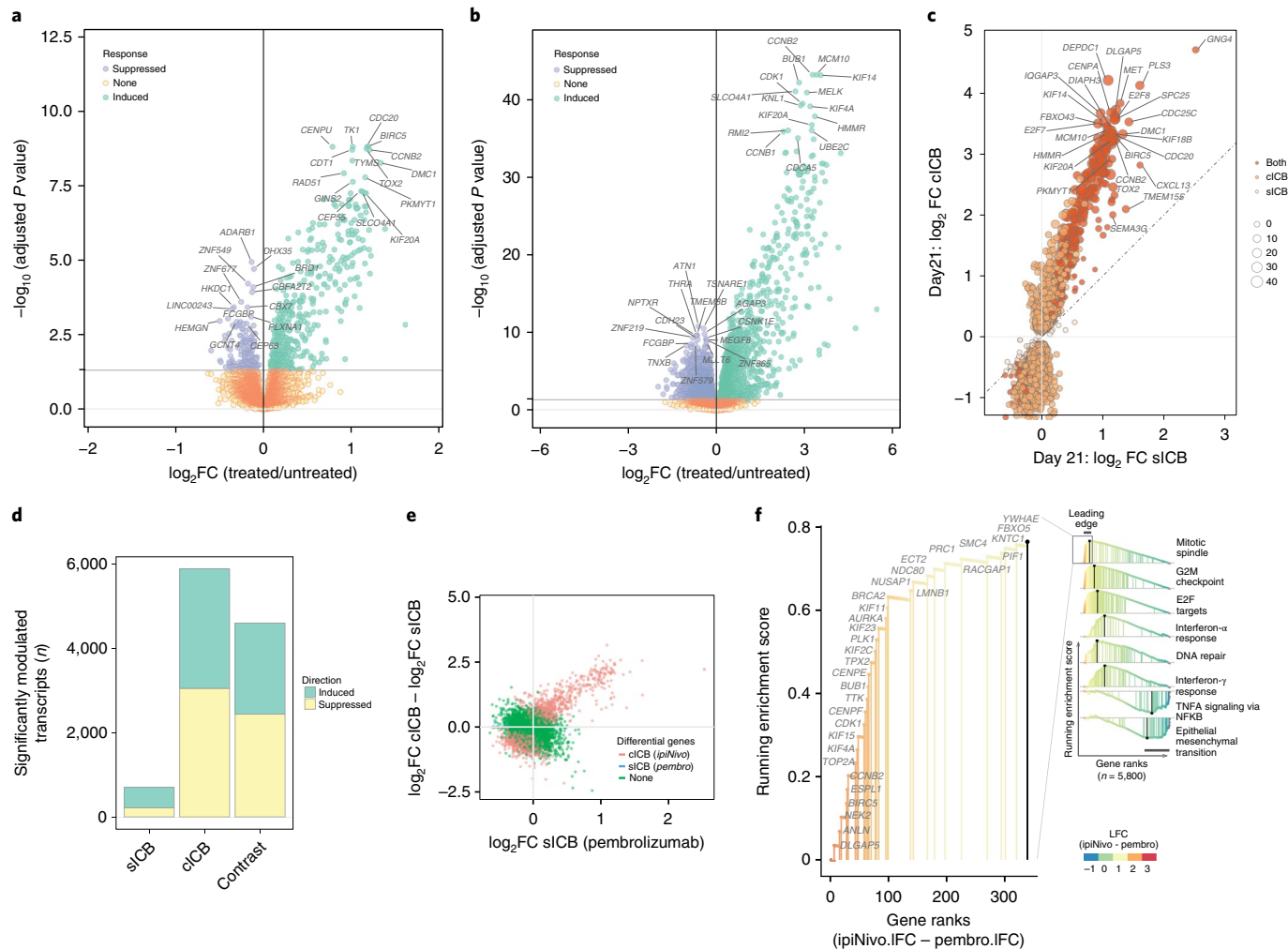


Fig. 1 | Transcriptomic response to ICB. **a**, Transcripts differentially regulated between pre-treatment and 21 d post-sICB (*n* = 40 paired samples, negative binomial Wald test, Benjamini-Hochberg corrected *P* values). **b**, cICB day 21 response (*n* = 15 paired samples, statistics as in **a**). **c**, log₂(fold change) (log₂FC) effect for sICB (*x* axis) versus cICB (*y* axis) for all transcripts significantly regulated in either treatment at day 21; size of points indicates *P*_{sICB}/*P*_{cICB}. **d**, Summary of transcript number modulated by each treatment and genes differentially expressed, comparing the response of cICB to sICB. **e**, Difference in log₂(fold change) (log₂FC) effect of cICB and sICB (*y* axis) versus log₂(fold change) of s-ICB (*x* axis). Each point represents a gene, with those in red having a significantly different effect size of treatment with cICB versus sICB genes. **f**, Rank-based gene set enrichment analysis of genes significantly more modulated by cICB identifies pathways preferentially induced or suppressed by combination treatment. LFC, log fold change.

M4 and M8, reflecting induction of cell division and mitochondrial translation (Extended Data Fig. 3).

To identify markers potentially informative for response to treatment, we performed differential expression analysis on CD8⁺ cell expression profiles on pre- and post-treatment samples from patients with cutaneous MM (144 samples from 69 patients, 67 pre-treatment and 77 post-treatment), controlling for age, treatment status and dichotomizing by 6-month clinical outcome. We identified 4,762 transcripts differentially expressed (FDR < 0.05) according to 6-month outcome (Fig. 2a and Supplementary Table 4). Genes associated with ongoing clinical response were distinct from those associated with ICB treatment, and induced pathways included positive regulation of viral transcription, mitochondrial translation, negative regulation of G2/M transition and T cell receptor (TCR) signaling. Durable clinical response was conversely associated with suppression of numerous pathways, including MAPKK activity and Toll-like receptor signaling (Fig. 2b). Given the wealth of transcript associations, we determined to define, in depth, the role of a robustly associated group of genes. We found 34 TRAV and TRBV transcripts, encoding TCR α - and β -chains, to be overexpressed in

responder samples (Fig. 2c). Furthermore, TCR-encoding genes were significantly over-represented among transcripts upregulated in responders, but not by ICB (odds ratio 4.4, *P* = 1.4 × 10⁻⁹; Fig. 2d). Thus differential expression of TCR-encoding genes is not a generalized response following ICB but, rather, corresponds to clinical outcome. To further understand this association, we mapped unbiased TCR repertoires from RNA-seq data using MiXCR¹⁷ to identify temporal changes in clonal composition (Fig. 2e). We found that cICB was associated with greater numbers of expanding clones on day 21 (Fig. 2f); after taking treatment into account, there was no association with age (*P* = 0.92) or sex (*P* = 0.18). To validate the accuracy of MiXCR in these samples, we performed quantitative PCR (qPCR) of peripheral blood mononuclear cell (PBMC) complementary DNA from 13 samples with TRA and TRB CDR3-specific primers designed to both stable and expanding clones (*n* = 52; Supplementary Table 5). This supported the MiXCR results, demonstrating a strong correlation between the inferred clonal frequency from RNA-seq and that derived from qPCR of PBMC (Extended Data Fig. 4). Modeling the transcriptional correlates of expanding clones in treated samples, and using the number of expanding clones

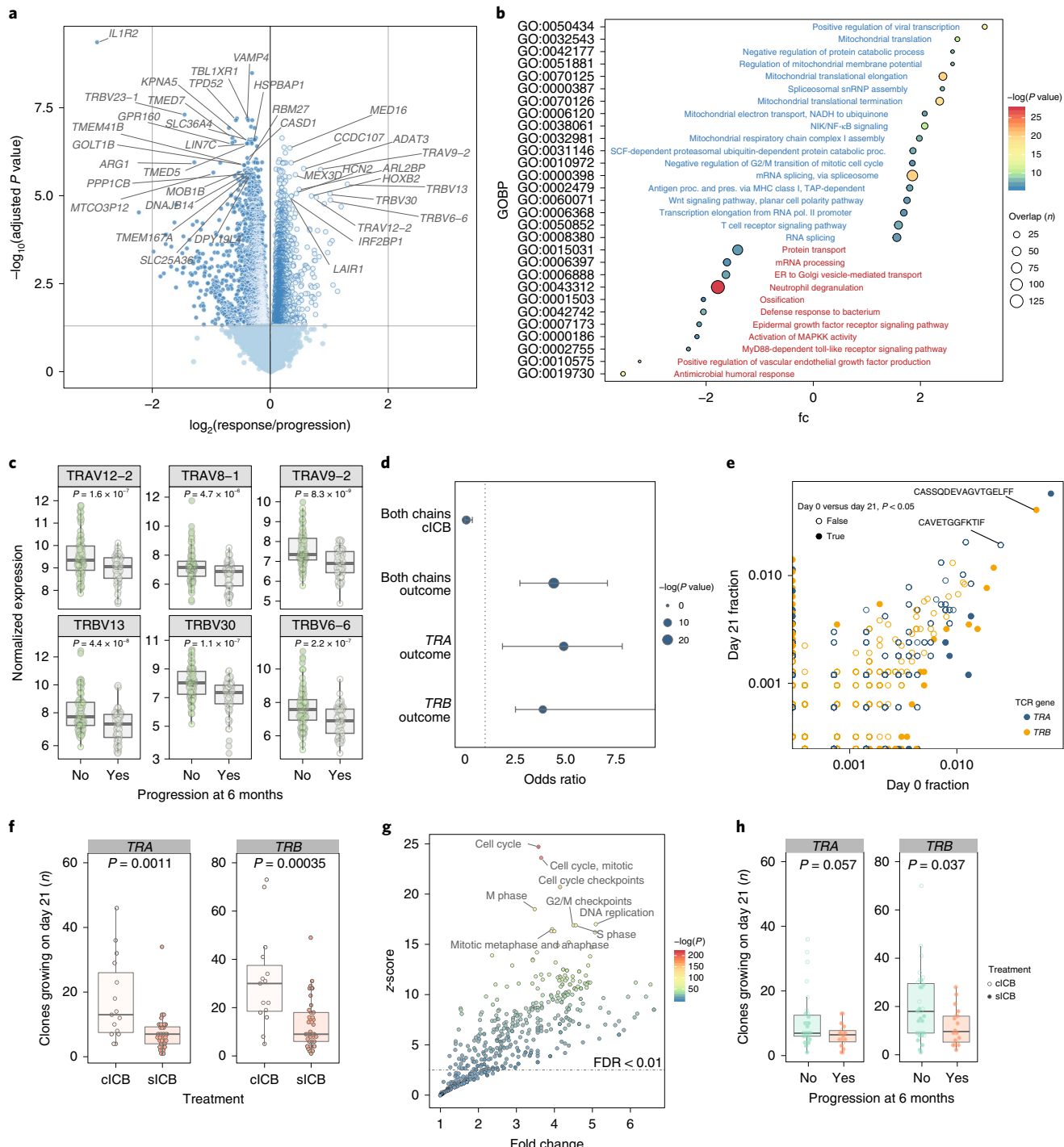


Fig. 2 | Identification of transcriptomic correlates of long-term response. **a**, Transcripts differentially regulated between responders and progressors, with direction showing relative expression in responders ($n=144$ samples from 69 patients, 67 pre-treatment and 77 post-treatment; negative binomial Wald test, Benjamini-Hochberg corrected P values). **b**, GOBP pathway analysis of genes preferentially upregulated (blue) and downregulated (red) in responders, Overlap (n), number of significant genes from a pathway (hypergeometric test).

c, Box plots of the most differentially regulated TCR genes between responders and progressors ($n=144$ samples, P values derived from uncorrected negative binomial Wald test returned from Deseq2).

d, Results from Fisher's exact test of enrichment of upregulated TCR encoding versus all transcripts, demonstrating no enrichment of TCR-encoding genes in those regulated by clICB, whereas both TRAV- and TRBV-encoding genes are highly enriched among those upregulated in responders (dotted line, odds ratio = 1; error bars, 95% confidence interval).

e, Representative example of day 0 versus day 21 clones from one patient showing both chains, with filled points representing clones showing significant change in frequency.

f, The number of clones increasing in size ($P < 0.05$) was significantly greater in clICB patients ($n=15$ clICB, $n=30$ sICB, two-sided Wilcoxon signed-rank test).

g, Reactome pathway analysis of genes positively associated with number of clones growing at day 21 ($n=54$) demonstrated increase in clone size to be strongly linked to expression of genes involved in mitosis (one-sided hypergeometric test of genes correlated with clone growth; Supplementary Table 6).

h, Number of clones growing at day 21 ($P < 0.05$) and outcome at 6 months ($n=49$ patients with cutaneous melanoma, two-sided Wilcoxon signed-rank test). Lower and upper hinges of boxes represent 25th to 75th percentiles, the central line represents the median, and the whiskers extend to highest and lowest values no greater than 1.5× interquartile range.

per sample as a continuous variable, we identified 3,502 transcripts associated with clonal growth (Supplementary Table 6). Genes linked to cell division and nucleic acid synthesis dominated those correlated to the number of expanding clones (Fig. 2g), validating the measure of clonal expansion by tracking TCR clones.

We further explored properties of the peripheral TCR repertoire, including clonal diversity, richness and clone size, for association with clinical outcome. We found no association with day 21 clonal diversity and clinical outcome at 6 months (Extended Data Fig. 5a), while the total number of expanding clones on day 21 was only marginally associated with oncological outcome at 6 months (Fig. 2h). These observations suggest that the associated TCR signal was instead contributed by a subset of cells. We noted that, post-treatment, responders tended to have more expanded clones than non-responders. Exploring this formally, we designated clones with count numbers $>0.5\%$ of the total number of clones per chain as 'large'. We found the number of large clones to be specifically higher on day 21 in responding patients compared to samples from either control subjects or non-responding patients ($P_{\text{versus control}} = 4.7 \times 10^{-5}$, $P_{\text{versus non-responders}} = 0.0015$; Fig. 3a). This observation held true if clones were identified by either TRA or TRB (Extended Data Fig. 5b). To explore the robustness of this observation, we recruited another cohort of 20 patients with MM and 43 healthy controls. With this group we similarly found that responding patients had more circulating large CD8⁺ clones than healthy controls ($P_{\text{versus control}} = 0.003$, $P_{\text{versus non-responders}} = 0.037$; Fig. 3b; combined Pvalues: control versus responder, $P = 2.4 \times 10^{-6}$; responder versus non-responder, $P = 6 \times 10^{-4}$). Across all day 21 cutaneous melanoma samples we found that the association between high clone count and 6-month outcome was independently significant across both sICB and cICB patient groups (Fig. 3c). To explore the effect of other covariates on this observation—namely age, total number of TCR identified (a reflection of sequencing depth), treatment type and sequencing run—we used a random effects model to test the relationship between day 21 large clone count and 6-month outcome¹⁸. This confirmed a highly significant association, with responders having on average 5.7 more large clones on day 21 (95% confidence interval: 2.6–8.7, $P = 4.8 \times 10^{-4}$; Supplementary Fig. 1). The 0.5% threshold size was most sensitive to differences between the two groups in both the original and replication cohorts, and showed suggestive association in baseline samples (Extended Data Fig. 5c). Kaplan–Meier estimates of both progression-free (Fig. 3d) and overall survival (Fig. 3e) were significantly different between patients, with day 21 large clone count below and above the median for the cohort. Analysis across all samples demonstrated no association between clinical outcome and the number of expanding clones (Extended Data Fig. 5d), or the cumulative clonal space occupied by large clones (Extended Data Fig. 5e), demonstrating that the absolute number of large clones, as opposed to the total proportion of the repertoire occupied, is of importance to outcome. While this effect was most evident post-treatment, when we increased power by pooling baseline samples across both cohorts and including those for which we did not have post-treatment samples ($n = 89$), we found pre-treatment large clone count similarly associated with outcome ($P = 0.006$, TRA; Extended Data Fig. 5f). Analysis of samples from 41 patients with data at baseline and at two further timepoints (taken at day 21 and before the fourth cycle of treatment—typically day 63) demonstrated that large clones show higher stability than other clone sizes (69.3% of those $>0.5\%$ of repertoire size remaining at day 63, versus 39.9% of clones 0.1–0.5% of repertoire size; Extended Data Fig. 6), illustrating a persistent presence in patient samples.

Human cytomegalovirus (CMV) leads to latent infection with profound effects on immune subset composition¹⁹ and hyper-expansion of memory T cell clones^{20,21}. Although the prevalence of CMV seropositivity markedly increases with age, any impact on ICB response is unknown. Given the association between early

clone size and outcome, we examined for a relationship with CMV seropositivity in 68 patients with samples available for serotyping. In keeping with memory cell inflation to a small number of antigens²⁰, CMV seropositivity was associated with increased counts of hyper-expanded clones ($>2\%$ of repertoire, $P = 1.1 \times 10^{-3}$, TRB, day 21 sample), with a concurrent depletion of smaller clones ($<0.01\%$, $P = 8 \times 10^{-5}$, TRB, day 21 sample; Extended Data Fig. 7a). This led to reduced TCR diversity per sample^{22,23} but, interestingly, no effect on large clone count or ICB outcomes was observed (Extended Data Fig. 7b–d). We examined public clonotypes reactive to either Epstein–Barr Virus (EBV), which shows ~95% seropositivity²⁴, or melanoma-associated antigens (MAA, Supplementary Table 7), to explore the effect of ICB treatment on clonotypes potentially related to, and independent of, melanoma. Whereas we found CD8⁺ TCR matching those recognizing MAA across patients and controls, clone sizes were larger in patients ($P = 2.8 \times 10^{-9}$; Extended Data Fig. 8a). The median clone size of EBV public clonotypes was also greater in patients with MM ($P = 0.001$), in keeping with observations of enlarged bystander clones in cancer²⁵ (Extended Data Fig. 8b). Consistent with both specific and generalized effects of ICB, treatment was associated with both larger EBV-reactive clones ($P = 0.0047$), and MAA-reacting clones ($P = 4.1 \times 10^{-5}$; Extended Data Fig. 8c,d). Where we had paired samples on days 21 and 63, we found that this increase persisted at the later timepoint (Extended Data Fig. 8e). It should be noted that most clonotypes have been characterized on HLA-A2-restricted antigens, whereas our analysis was independent of HLA type. However, the analysis of clonal expansion was paired and significant variation between control and patient human leukocyte antigen (HLA) status is unanticipated. Notably, eight patients had one or more large clones matching known MAA clonotypes from this small subset of public clonotypes, indicating that large clones frequently recognize known melanoma antigens.

To explore associations between large clone count and CD8⁺ T cell subset composition, we performed flow cytometry on PBMC samples taken before and during treatment ($n = 42$ samples, $n = 19$ patients), assessing the number of naïve (T_N), central (T_{CM}) and effector memory (T_{EM}), and effector memory re-expressing CD45RA (T_{EMRA}) cells, in CD3⁺CD8⁺ cells gated according to the expression of CD27 and CD45RA (Supplementary Fig. 2). Integrating these data demonstrated that clonal diversity was highly correlated with T_{CM} counts and anti-correlated with T_{EMRA} counts (Extended Data Fig. 9a). We found a strong association between large clone count and CD8⁺ T_{EM} counts from the same samples ($r = 0.59$, $P = 3.4 \times 10^{-5}$). Large clone count was conversely weakly anti-correlated with counts of both CD8⁺ T_N and T_{EMRA} (Fig. 3f). However, there was no association between CD4⁺ T cell subset percentages and large clone count, confirming the specificity of our findings to CD8⁺ T cells (Extended Data Fig. 9b).

Finally, we explored whether combining module gene expression data, patient baseline hematology parameters and large clone count might predict patient outcomes. We identified ten variables that can be incorporated through linear discriminant analysis to build a predictive model of 6-month clinical outcome with favorable receiver operating characteristics (ROC) (area under the curve = 0.823; Supplementary Fig. 3a). Our findings highlight the potential importance of these observations for patient care and, crucially, substantiate large clone count as the most important informative predictor (Supplementary Fig. 3b). Given this, and the cytometry data inferring that large clones have an effector-like phenotype, we used 5' single-cell RNA-seq to further dissect the transcriptional properties of large clones.

Clustering of expression profiles from post-ICB CD8⁺ T cells (patient numbers: $n = 4$ sICB and $n = 4$ cICB) identified four distinct subsets. The first two of these, Clusters 1 and 2, displayed effector-like patterns and both strongly expressed GZMK, a marker of early exhaustion^{12,26}. Cluster 1 additionally had other markers of

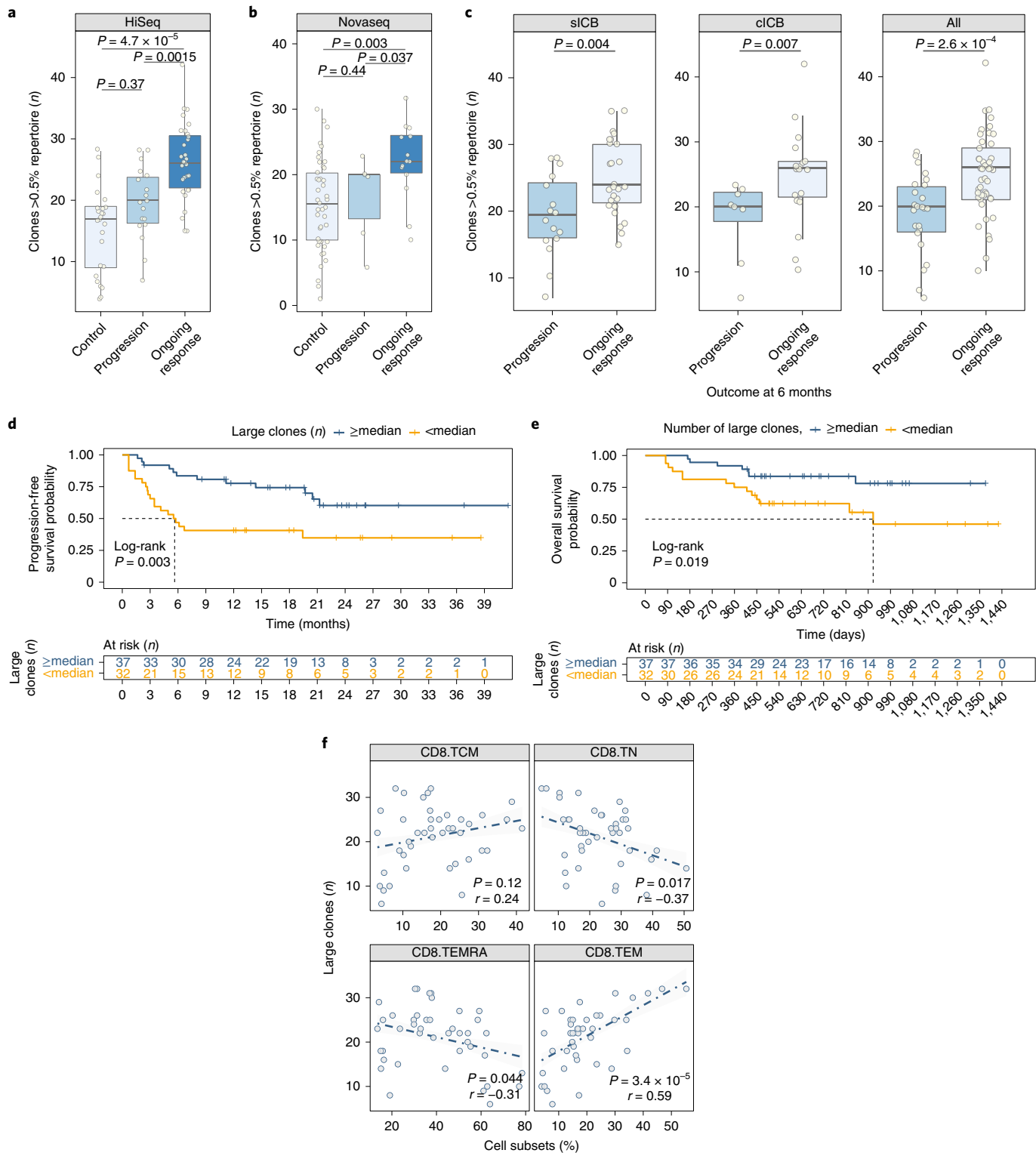


Fig. 3 | Number of large clones is of prognostic importance. **a**, Number of clones >0.5% of repertoire at day 21 is significantly greater in responding patients than in control samples (clones identified by TRA chain, $n=25$ controls, $n=49$ patients, two-sided Wilcoxon signed-rank test; lower and upper box hinges represent the 25th to 75th percentiles, the central line represents the median and the whiskers extend to the highest and lowest values no greater than $1.5 \times$ interquartile range). **b**, Replication cohort ($n=43$ controls, $n=20$ patients, one-sided Wilcoxon signed-rank test, box plot as in **a**). **c**, Day 21 large clone count is associated with 6-month outcomes after sICB (left, $n=42$), cICB (center, $n=27$) and when considering all ICB (right, $n=69$; P values all derived from one-sided Wilcoxon signed-rank test, box plot as in **a**). **d**, Shorter progression-free survival in patients with day 21 large clone count below median versus those with count above ($P=0.003$, two-sided log-rank test, $n=69$). **e**, Kaplan-Meier survival curve demonstrating reduced overall survival in patients with day 21 large clone count below median versus those with count above ($P=0.01$, two-sided log-rank test, $n=69$). **f**, Correlation between large clone count and cell subset percentages (TCM, central memory; TN, naive; TEMRA, effector memory re-expressing CD45RA; TEM, effector memory) from flow cytometry ($n=42$ samples, $n=19$ patients, r denotes Pearson correlation, P values obtained from two-sided t-tests).

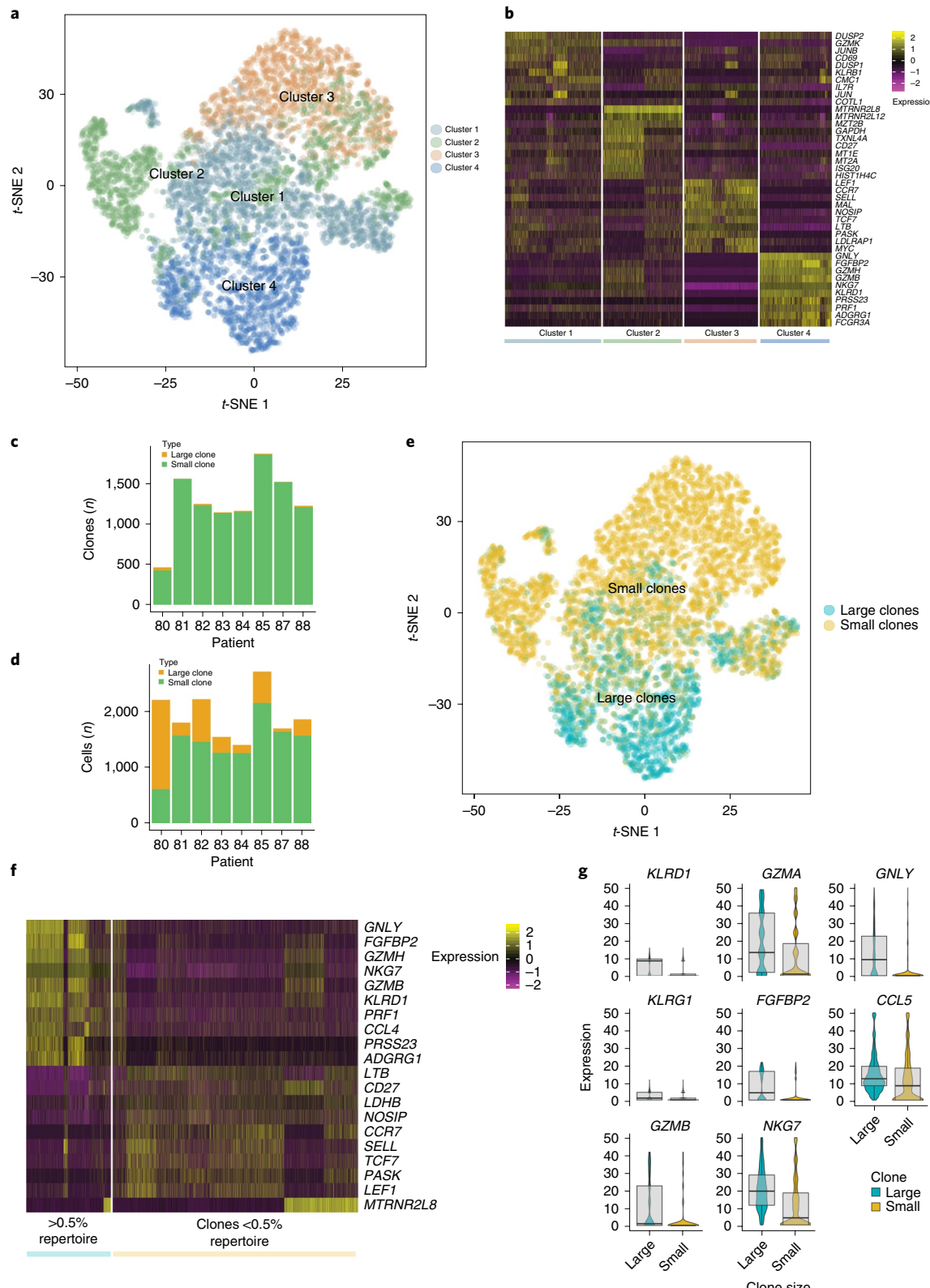


Fig. 4 | Single-cell sequencing demonstrates that large clones have a distinct cytotoxic expression profile. **a**, Plot of *t*-distributed stochastic neighbor-embedding (*t*-SNE) for post-treatment CD8⁺ cell expression profiles from $n=8$ individuals (patient numbers: $n=4$ sICB and $n=4$ ICB; $n=12,699$ cells), with color coding indicating cell clusters as identified by canonical correlation analysis. **b**, Heatmap of genes differentially expressed according to cluster identity as in **a**. **c**, Bar plot demonstrating total number of clones per sample (large clones >0.5% of repertoire). **d**, Numbers of cells belonging to small (green) and large clones per sample. **e**, *t*-SNE as in **a**, but cells are now color coded according to whether they belong to large or small clones. **f,g**, Heatmap (**f**) and box plots (**g**) demonstrating genes most significantly differentially expressed between large and small clones (lower and upper box hinges represent 25th to 75th percentiles, central line the median and the whiskers extend to highest and lowest values no greater than 1.5× interquartile range; the violin component refers to the kernel probability density and encompasses all cells).

activation, cytotoxicity and exhaustion (for example, *CD69*, *KLRB1* and *TIGIT*), while Cluster 2 was further distinguished by the expression of *CD27* and markers of active mitosis (for example, *MZT2A* and *MZT2B*; Fig. 4a,b and Supplementary Table 8). The other clusters displayed expression profiles indicative of naïve (Cluster 3: *LEF1*, *TCF7* and *CCR7*) and effector memory (Cluster 4: *GNLY*, *FGFBP2* and *GZMH*) phenotypes.

Having defined clone size by the number of copies of distinct β -chains, we explored how gene expression profiles at the single-cell level differ as a function of clonal size post-ICB. The inferred clonal frequency was remarkably similar to that from the matched clones for these samples from bulk (Extended Data Fig. 10a–h). Clones were labeled as large or small according to the 0.5% repertoire threshold per individual, with a significant correlation between the number of large clones identified in single-cell and bulk data (Extended Data Fig. 10i). The numbers of large clones per individual, and their respective contribution to the clonal space, were highly variable (Fig. 4c,d). Strikingly, we found large clones clustered together, predominantly composed of cells from Cluster 4 but with a contribution from Cluster 1, indicating a shared expression profile (Fig. 4e). Performing differential expression analysis on large clones versus all others revealed that cells from large clones have a uniquely cytotoxic profile, with high expression of *CCL4*, *PRF1* and *GNLY* among other genes (Fig. 4f and Supplementary Table 9). It has recently been demonstrated that expression of *ITGB1*, encoding CD29, defines a uniquely cytotoxic subset of CD8⁺ T cells with enhanced cytolytic activity²⁷, and we note that *ITGB1* is a key marker gene for large clones in our dataset.

In summary, we present a large transcriptomic analysis of peripheral CD8⁺ lymphocytes across a cohort of patients with MM receiving ICB. We show that treatment results in induction of distinct modules of genes, most notably those involved in cell division, but this does not directly correlate with patient outcome. Rather, early samples from responding patients demonstrate overexpression of TCR-encoding genes, and this is associated with having a greater number of discrete large clones in the circulating repertoire. A strength of the observed novel relationship between day 21 large clone count and outcome is that it is agnostic to the clone target. This is important, because T cell clonal targets will vary markedly within and between individuals and thus a generalized peripheral marker is required for translation to patient care. Nonetheless, the precise specificity of T cell clones is of importance in immunotherapy, and understanding whether large clones are enriched for those specific for tumor antigens will be of interest. Notably, large clones have a distinct cytotoxic gene expression profile, inferring activity and the underlying basis with long-term clinical response. Future work will explore the association between HLA type and clonal architecture, as well as regulatory polymorphisms in determining ICB response. In addition to providing insights into the dynamics of the response to ICB, our study illustrates the power of combining transcriptomics with TCR analysis across large cohorts to determine long-sought predictive markers of durable clinical benefit from ICB.

Online content

Any methods, additional references, Nature Research reporting summaries, source data, extended data, supplementary information, acknowledgements, peer review information; details of author contributions and competing interests; and statements of data and code availability are available at <https://doi.org/10.1038/s41591-019-0734-6>.

Received: 29 October 2019; Accepted: 9 December 2019;

Published online: 10 February 2020

References

- Tumeh, P. C. et al. PD-1 blockade induces responses by inhibiting adaptive immune resistance. *Nature* **515**, 568–571 (2014).
- Pan, D. et al. A major chromatin regulator determines resistance of tumor cells to T cell-mediated killing. *Science* **359**, 770–775 (2018).
- Miao, D. et al. Genomic correlates of response to immune checkpoint blockade in microsatellite-stable solid tumors. *Nat. Genet.* **50**, 1271–1281 (2018).
- Davoli, T., Uno, H., Wooten, E. C. & Ellledge, S. J. Tumor aneuploidy correlates with markers of immune evasion and with reduced response to immunotherapy. *Science* **355**, eaaf8399 (2017).
- Daud, A. I. et al. Programmed death-ligand 1 expression and response to the anti-programmed death 1 antibody pembrolizumab in melanoma. *J. Clin. Oncol.* **34**, 4102–4109 (2016).
- Brochez, L. et al. Challenging PD-L1 expressing cytotoxic T cells as a predictor for response to immunotherapy in melanoma. *Nat. Commun.* **9**, 2921 (2018).
- Jacquelot, N. et al. Predictors of responses to immune checkpoint blockade in advanced melanoma. *Nat. Commun.* **8**, 592 (2017).
- Krieg, C. et al. Author correction: high-dimensional single-cell analysis predicts response to anti-PD-1 immunotherapy. *Nat. Med.* **24**, 1773–1775 (2018).
- McQuade, J. L. et al. Association of body-mass index and outcomes in patients with metastatic melanoma treated with targeted therapy, immunotherapy, or chemotherapy: a retrospective, multicohort analysis. *Lancet Oncol.* **19**, 310–322 (2018).
- Kugel, C. H. et al. Age correlates with response to anti-PD1, reflecting age-related differences in intratumoral effector and regulatory T-cell populations. *Clin. Cancer Res.* **24**, 5347–5356 (2018).
- Blank, C. U., Haanen, J. B., Ribas, A. & Schumacher, T. N. The ‘cancer immunogram’. *Science* **352**, 658–660 (2016).
- Huang, A. C. et al. T-cell invigoration to tumour burden ratio associated with anti-PD-1 response. *Nature* **545**, 60–65 (2017).
- Wang, W. et al. Biomarkers on melanoma patient T cells associated with ipilimumab treatment. *J. Transl. Med.* **10**, 146 (2012).
- Das, R. et al. Combination therapy with anti-CTLA-4 and Anti-PD-1 leads to distinct immunologic changes in vivo. *J. Immunol.* **194**, 950–959 (2015).
- Langfelder, P. & Horvath, S. WGCNA: an R package for weighted correlation network analysis. *BMC Bioinformatics* **9**, 559 (2008).
- Russo, P. S. T. et al. CEMiTTool: a Bioconductor package for performing comprehensive modular co-expression analyses. *BMC Bioinformatics* **19**, 56 (2018).
- Bolotin, D. A. et al. MiXCR: software for comprehensive adaptive immunity profiling. *Nat. Methods* **12**, 380–381 (2015).
- Bates, D., Mächler, M., Bolker, B. & Walker, S. Fitting linear mixed-effects models using lme4. Preprint at <https://arxiv.org/abs/1406.5823> (2014).
- The Milieu Intérieur Consortium et al. Natural variation in the parameters of innate immune cells is preferentially driven by genetic factors. *Nat. Immunol.* **19**, 302–314 (2018).
- Weekes, M. P., Wills, M. R., Mynard, K., Carmichael, A. J. & Sissons, J. G. The memory cytotoxic T-lymphocyte (CTL) response to human cytomegalovirus infection contains individual peptide-specific CTL clones that have undergone extensive expansion in vivo. *J. Virol.* **73**, 2099–2108 (1999).
- Gillespie, G. M. A. et al. Functional heterogeneity and high frequencies of cytomegalovirus-specific CD8⁺ T lymphocytes in healthy seropositive donors. *J. Virol.* **74**, 8140–8150 (2000).
- Suessmuth, Y. et al. CMV reactivation drives posttransplant T-cell reconstitution and results in defects in the underlying TCR- β repertoire. *Blood* **125**, 3835–3850 (2015).
- Wang, G. C., Dash, P., McCullers, J. A., Doherty, P. C. & Thomas, P. G. T. Cell receptor diversity inversely correlates with pathogen-specific antibody levels in human cytomegalovirus infection. *Sci. Transl. Med.* **4**, 128ra42 (2012).
- Durovic, B. et al. Epstein–Barr virus negativity among individuals older than 60 years is associated with HLA-C and HLA-Bw4 variants and tonsillectomy. *J. Virol.* **87**, 6526–6529 (2013).
- Simoni, Y. et al. Bystander CD8⁺ T cells are abundant and phenotypically distinct in human tumour infiltrates. *Nature* **557**, 575–579 (2018).
- Zheng, C. et al. Landscape of infiltrating T cells in liver cancer revealed by single-cell sequencing. *Cell* **169**, 1342–1356.e16 (2017).
- Nicolet, B. P. et al. CD29 marks superior cytotoxic human T cells. Preprint at *bioRxiv* <https://doi.org/10.1101/562512> (2019).

Publisher's note Springer Nature remains neutral with regard to jurisdictional claims in published maps and institutional affiliations.

© The Author(s), under exclusive licence to Springer Nature America, Inc. 2020

Methods

Sample collection. Patients provided written informed consent to donate samples for analysis to the Oxford Radcliffe Biobank (Oxford Centre for Histopathology Research ethical approval nos. 16/A019 and 18/A064); 30–50 ml blood was collected into EDTA tubes (BD vacutainer system) taken immediately pre-treatment, at day 21, and before the fourth cycle of treatment (day 63). Due to logistical issues and delays with treatment, some day 63 samples were taken later but before the fifth cycle (Supplementary Table 1). Control samples were collected via the Oxford Biobank (www.oxfordbiobank.org.uk) with full ethical approval (no. REC 06/Q1605/55), and with written informed consent from healthy volunteers of European ancestry between the ages of 24 and 61 years (median, 49.5 years; interquartile range (IQR), 34–54 years). Peripheral blood mononuclear cells were obtained by density centrifugation (Ficoll Paque). CD8⁺ cell isolation was carried out by positive selection (Miltenyi) according to the manufacturer's instructions, with all steps performed either at 4 °C or on ice.

Treatment outcomes. All samples were obtained from patients receiving standard of care treatment within the UK's National Health Service (NHS), and outcomes were defined either clinically or using radiological assessment according to irRECIST 1.1, performed approximately 12 and 24 weeks post-initiation of treatment. Progressors were defined as those with radiographic disease progression at either of these two timepoints, or who had unequivocal rapid disease progression necessitating cessation of ICB treatment. Outcomes were dichotomized according to evidence of radiological disease stability or response for the minimum duration of 24 weeks, per Roh et al.²⁸. Although 78 samples had pre- and post-treatment data for analysis of correlates of outcome, mucosal, small cell and uveal melanoma showed reduced sensitivity to immunotherapy and dissimilar clinical behavior, and hence these samples ($n=8$ individuals) were excluded from analysis of clinical outcomes. In a further patient, a review of the radiology suggested that disease was not-metastatic post-treatment and those data were similarly excluded (Supplementary Table 1).

RNA extraction. Post-selection cells were spun down and resuspended in 350 µl of RLTPplus buffer with 1% beta-mercaptoethanol or DTT, and transferred to 2-ml tubes. Samples were stored at –80 °C for batched RNA extraction. Homogenization of the sample was carried out using the QIAshredder (Qiagen). The AllPrep DNA/RNA/miRNA kit (Qiagen) was used for RNA extraction. DNaseI was used during the extraction protocol to minimize DNA contamination. RNA was eluted into 35 µl of RNase-free water. The amount of RNA present was quantified by Qubit analysis, and RNA samples stored at –80 °C until ready for sequencing.

RNA-seq. Poly(A) RNA was, for the original cohort, 75-base pair-end sequenced on Illumina HiSeq-4000 machines and, for the replication cohort, 150-base pair-end sequenced on an Illumina Novaseq, both at the Oxford Genome Centre, Wellcome Centre for Human Genetics. Reads were aligned to CRGh38/hg38 using HISAT2 (ref. ²⁹), and read count information was generated using HTSeq³⁰. High-mapping quality reads were selected based on MAPQ score using bamtools. Marking and removal of duplicate reads were performed using picard (v.1.105), and samtools was used to pass through the mapped reads and calculate statistics³¹. In total, 297 high-quality transcriptomes (properly paired, 14,080,086,168 reads; median per sample, 47,490,000) were selected and used for downstream analysis. We detected potential sample contamination and swaps using verifyBamID³², and four samples with >2.5% were excluded from outcome analysis (Supplementary Table 1). We applied DESeq2 (v.1.18.1) to produce normalized counts³³.

TCR mapping. MiXCR was used to map reads on reference sequences of V, D and J genes, and to quantitate TCR clonotypes from mapped reads using complementarity-determining region 3 (CDR3) gene regions¹⁷. The non-default partial alignments option (OallowPartialAlignments = true) was applied to preserve partial alignments for the assembly step. We performed three iterations of read assembly to increase the number of assembled reads containing the CDR3 region using assemblePartial action. Position quality scores were used to switch on the frequency-based correction of clonotype assembling and clustering (ObadQualityThreshold=15). Clones were called according to the CDR3 nucleotide sequence. We identified a median of 1,007 α (IQR, 635–1,319) and 1,619 β (IQR, 957–2,247) unique chains per sample from the HiSeq dataset, and 1,562 α (IQR, 889–1,983) and 2,159 β (IQR, 1,310–2,718) unique chains per sample from the Novaseq data. Information about clonotypes was extracted with default parameters and processed in R, and clonal indices were calculated using the vegan package³⁴. For each sample we determined the total number of clones mapped separately per TCR gene (TRA and TRB), and expressed individual clone sizes as a proportion of this total number.

Differential gene expression. DESeq2 (ref. ³³) was used for differential expression analysis. For comparison of baseline versus day 21 expression, we used a pairwise approach controlling for the individual. Only transcripts with mean count number >10 were analyzed, using the binomial Wald test with 750 iterations after correcting for size factors and dispersion. To explore significant differences between sICB and cICB responses, we tested for an interaction between treatment and type.

To identify genes differentially expressed between progressors at 6 months and those with continued benefit of treatment, we considered only transcripts with >50 read counts and used age and whether the sample was pre- or post-treatment as covariates. Identification of transcripts associated with clone growth was performed over $n=54$ day 21 samples by testing the number of transcripts associated with clone growth. Clones were defined by β -chain and were identified as growing if they were enlarged at baseline ($P < 0.001$, Fisher's exact test).

Identification of ICB-regulated modules. To increase the observation of ICB-responsive genes with higher inter-individual variation, we analyzed transcripts showing response to one or both treatments at FDR < 0.05 ($n=7,329$ transcripts). Normalized expression data for all 191 samples (control samples from $n=22$ individuals plus $n=169$ patient samples) were extracted for these genes and co-expressed modules discovered from the data matrix using CEMiTTool in R¹⁶, with the following settings: filter = FALSE, merge_similar = TRUE, min_ngen = 80. Modules of genes were extracted and pathway analysis performed.

Pathway analysis and gene set enrichment. Pathway analysis was performed using the R package XGR³⁵ using the GOBP and Reactome databases. Induced and suppressed transcripts were analyzed separately against the background of all tested transcripts. The default ontology algorithm was used ('none') and a hypergeometric test employed. To identify pathways most differentially regulated between sICB and cICB, genes were ranked in order of differential induction and gene set enrichment analysis was performed with the R package P1³⁶ using the MsigdbH ontology and pathways containing 20–5,000 genes, with 20,000 permutations used.

qPCR. In total, 1.25 million PBMCs were lysed in 350 µl of RLT buffer (Qiagen) supplemented with 1% beta-mercaptoethanol or DTT. RNA was extracted from PBMC samples using QIAshredder and AllPrep DNA/RNA/miRNA Universal Kits (Qiagen). Eight microliters of RNA was reverse transcribed using the SuperScript III First-Strand Synthesis System (Thermo Fisher Scientific). MIXCR data were validated by correlating TCR clonal expansion 21 d post-ICB treatment by qPCR with predicted clonal expansion using MIXCR data. TRA and TRB chains were targeted in both expanding and unchanged control clones in a patient-specific manner. Clones were selected based on clonal size and significance of expansion post-ICB treatment. Primers were designed to selectively amplify CD8⁺ TCR clones, with the forward primer targeting the CDR3 region and the reverse targeting the TCR constant region. Melt curves were performed to optimize primer specificity. PCR reactions (10 µl) were performed in duplicate per sample using 5 µl of iTaq Universal SYBR Green Supermix (Bio-Rad), 0.8 µl of 5 µM primers (forward and reverse) and 4.2 µl of cDNA (diluted in nuclease-free water) per reaction. A holding stage of 95 °C for 10 min was applied before PCR cycling: 95 °C for 15 s and 63 °C for 60 s for 40 cycles. The delta-delta threshold cycle method was used to calculate relative expression and fold change of genes in paired untreated and day 21 samples. Threshold cycle values were normalized to CD3E to account for the T cell proportion of PBMCs.

Flow cytometry. After processing, PBMCs were resuspended in freezing media (10% DMSO, 90% FBS) and stored in liquid nitrogen. For flow cytometry analysis, 1×10^6 cells were stained in HBSS supplemented with 5% FBS in the dark, on ice, for 30 min before fixation in 2% formaldehyde. All samples were also stained using a fixable amine reactive viability dye (LIVE/DEAD Fixable Near-IR Dead Cell Stain Kit). Staining antibodies, clones and manufacturer details are shown in Supplementary Fig. 2. Flow cytometry was performed using an LSRII (Becton Dickinson), and FlowJo software (Treestar) was used for analysis. When exploring associations with large clone count, flow cytometry and FlowJo analysis was performed blinded to bioinformatic and clinical data.

Identification and combination of informative predictors in patient response prediction. Based on transcriptomic and clinical data obtained in this study, we constructed three types of predictor: (1) module hub genes ('hub1'–'hub9'; lead hub gene per module identified from transcriptome data); (2) clone-derived features, that is, large count on day 21 of treatment and total large count (sum of pre- and post-treatment); and (3) cell counts of neutrophils and monocytes ('neut' and 'mono'). We first applied random forest (RF, R package randomForest, v.4.6–14) to estimate the relative importance of predictors considered. For model building, we used fivefold cross-validation (repeated ten times) to find the best model with optimal parameters tuned. Based on the built RF model, we measured the importance of a predictor by the degree of decrease in accuracy after removal of that predictor (this measure is more robust than direct measurement of a predictor by its predictive power). A high score in accuracy indicates a highly informative predictor. We next applied linear discriminant analysis (R package MASS, v.7.3–51.4) to combine all identified informative predictors. We calculated linear discriminant scores used for patient response prediction. Linear discriminant scores are a linear combination of predictors (thus with better prediction explanations); the performance (measured by area under the curve) of such combinations was compared to prediction using individual predictors alone.

Single-cell RNA-seq. Samples were obtained after the first treatment cycle (day 21). Following isolation of PBMC subsets (see Sample collection), CD8⁺ and CD14⁺ cells ($n = \sim 12,000$) were combined in suspension. Single cells were isolated using oil-droplet partitioning and tagged with a unique barcode per the Chromium system (10x Genomics, Chromium Single Cell V(D)J and 5' Library kits). Reverse transcription, amplification and library preparation of both 5' transcriptome and V(D)J libraries were performed per published protocols (10x Genomics). The library was sequenced using a HiSeq platform at a minimum of 50,000 reads per cell (data presented—60,470 reads per cell).

Data processing. Cellranger (v.3.0.2) mkfastq was applied to the Illumina BCL output to produce FASTQ files. Cellranger count was then applied to each FASTQ file to produce a feature barcoding and gene expression library. Cellranger aggr was used to combine samples for merged analysis.

Quality control. We applied the *scater* package to filter out single-cell profiles that were outliers for any metric as low-quality libraries³⁷. We used size factors to scale the normalization of cell-specific biases and used log-normalized expression values for downstream use³⁸. Technical noise was modeled using the *scran* package³⁹ based on the optimal number of principal components⁴⁰. The *scran* package was applied to detect and remove doublets using the expression profiles⁴¹.

Modeling and comparison of small and large TCR clonotypes. Subsetting was performed to select cells expressing *CD8A*, *CD8B* and *CD3D*. Further subsetting excluded residual cells expressing *CD14* or *CD19*. A canonical correlation analysis was run with 20 canonical clusters selected for downstream analysis using the Seurat package⁴². An integrated analysis of all merged data was performed using defined canonical clusters. Following identification of cellular subgroups based on TCR clonotype, conserved markers defining subgroups were identified using the FindMarkers function with a default two-sided Wilcoxon rank-sum test. Plots were generated using ggpubr (v.0.2) and customizing ggplot2.

General statistical analysis. Statistical tests performed are stated for each figure, the analysis was performed using R v.3.4.3 (Kite-Eating Tree) and figures made with ggplot2. Lme4 (ref. ⁴³) was used for the linear random effects model. P-values were combined using Fisher's method. The lower and upper box hinges on box plots represent 25th to 75th percentiles, central line the median and the whiskers extend to largest and smallest values no greater than 1.5 \times interquartile range.

Further information on experimental design and statistical analyses is available in the Nature Research Reporting Summary linked to this article.

Reporting Summary. Further information on research design is available in the Nature Research Reporting Summary linked to this article.

Data availability

All sequencing data will be made freely available to organizations and researchers to conduct research in accordance with the UK Policy Framework for Health and Social Care Research via a data access agreement. Sequence data have been deposited at the European Genome–phenome Archive, which is hosted by the European Bioinformatics Institute and the Centre for Genomic Regulation under accession no. EGAS00001004081. Patient anonymized raw flow cytometry data are freely accessible for download from the group bitbucket account.

Code availability

Scripts used in the analysis and figure synthesis are available from the Fairfax group bitbucket account: <https://bitbucket.org/Fairfaxlab/identification-of-peripheral-cd8-t-cell-subsets-associated/src/master/>

References

28. Roh, W. et al. Integrated molecular analysis of tumor biopsies on sequential CTLA-4 and PD-1 blockade reveals markers of response and resistance. *Sci. Transl. Med.* **9**, eaah3560 (2017).
29. Kim, D., Langmead, B. & Salzberg, S. L. HISAT: a fast spliced aligner with low memory requirements. *Nat. Methods* **12**, 357–360 (2015).
30. Anders, S., Pyl, P. T. & Huber, W. HTSeq—a Python framework to work with high-throughput sequencing data. *Bioinformatics* **31**, 166–169 (2015).
31. Li, H. et al. The sequence alignment/Map format and SAMtools. *Bioinformatics* **25**, 2078–2079 (2009).
32. Jun, G. et al. Detecting and estimating contamination of human dna samples in sequencing and array-based genotype data. *Am. J. Hum. Genet.* **91**, 839–848 (2012).
33. Love, M. I., Huber, W. & Anders, S. Moderated estimation of fold change and dispersion for RNA-seq data with DESeq2. *Genome Biol.* **15**, 550 (2014).
34. Dixon, P. VEGAN, a package of R functions for community ecology. *J. Veg. Sci.* **14**, 927–930 (2003).
35. Fang, H., Knezevic, B., Burnham, K. L. & Knight, J. C. XGR software for enhanced interpretation of genomic summary data, illustrated by application to immunological traits. *Genome Med.* **8**, 129 (2016).
36. The ULTRA-DD Consortium et al. A genetics-led approach defines the drug target landscape of 30 immune-related traits. *Nat. Genet.* **51**, 1082–1091 (2019).
37. McCarthy, D. J., Campbell, K. R., Lun, A. T. L. & Wills, Q. F. Scater: pre-processing, quality control, normalization and visualization of single-cell RNA-seq data in R. *Bioinformatics* **8**, 1179–1186 (2017).
38. Lun, A. T., Bach, K. & Marioni, J. C. Pooling across cells to normalize single-cell RNA sequencing data with many zero counts. *Genome Biol.* **17**, 75 (2016).
39. Huber, W. et al. Orchestrating high-throughput genomic analysis with Bioconductor. *Nat. Methods* **12**, 115–121 (2015).
40. Lun, A. T. L., McCarthy, D. J. & Marioni, J. C. A step-by-step workflow for low-level analysis of single-cell RNA-seq data with Bioconductor. *F1000Res.* **5**, 2122 (2016).
41. Dahlin, J. S. et al. A single-cell hematopoietic landscape resolves 8 lineage trajectories and defects in Kit mutant mice. *Blood* **131**, e1–e11 (2018).
42. Stuart, T. et al. Comprehensive integration of single-cell data. *Cell* **177**, 1888–1902.e21 (2019).

Acknowledgements

We are very grateful to all patients who generously contributed samples and participated in the study. We thank all the staff of the Day Treatment Unit, Oxford Cancer Centre, and N. Coupe and R. Matin for assistance in collecting patient samples. We thank R. Morgan for discussion and advice. This study was funded by a Wellcome Intermediate Clinical Fellowship to B.P.F. (no. 201488/Z/16/Z), additionally supporting E.A.M. and I.N. R.A.W. was a National Institute for Health Research (NIHR) Academic Clinical Fellow and was supported by a CRUK predoctoral Fellowship (no. ANR00740). R.C. is supported by a CRUK Clinical Research Training Fellowship. C.A.T. is funded by the Engineering & Physical Sciences Research Council and the Balliol Jowett Society (no. D4T00070). J.C.K. is funded by a Wellcome Trust Investigator Award (no. 204969/Z/16/Z). P.K. is supported by a NIHR Senior Fellowship and Wellcome Trust Award (no. WT109965MA). V.W. was supported by a CRUK CTAAC Clinical Trials Fellowship (no. C2195/A19716), and also by the NIHR Oxford Biomedical Research Centre. The views expressed are those of the authors and not necessarily those of the NHS, the NIHR or the Department of Health.

Author contributions

M.R.M. initiated the cohort. B.P.F. conceived and supervised the study. B.P.F. with contributions from C.A.T., I.N., R.A.W., H.F., M.H.A.-M., P.K. and M.R.M., drafted the paper and figures. B.P.F. and I.N. carried out the primary analysis. M.P., V.W., B.P.F., M.R.M. and R.A.W. carried out patient recruitment. S.D., E.A.M., R.A.W., R.C., C.A.T. and B.P.F. collected samples and purified cells. S.D. and E.A.M. extracted RNA. I.N. provided RNA-seq pipelines, quality control and bioinformatics support. C.A.T. carried out flow cytometry and qPCR clones. R.A.W., R.C. and I.N. carried out single-cell sequencing. Z.T. provided the radiological reporting. R.A.W. and B.P.F. collated the clinical data. H.F. and J.C.K. provided statistical support and machine learning. J.C.K. provided scientific and infrastructural support. All authors reviewed and edited the final paper.

Competing interests

M.H.M. reports personal fees from Amgen, grants and personal fees from Roche, grants from Astrazeneca, grants and personal fees from GSK, personal fees and other from Novartis, other from Millenium, personal fees, non-financial support and other from Immunocore, personal fees and other from BMS, personal fees and other from Eisai, other from Pfizer, personal fees, non-financial support and other from Merck/MSD, personal fees and other from Rigontec (acquired by MSD), other from Regeneron, personal fees from BiolineRx, personal fees and other from Array Biopharma (now Pfizer), non-financial support and other from Replimune, outside the submitted work. M.P. has received support with conference travel, and fees for advisory work and speaking from Amgen, BMS, L'Oreal, MSD, Novartis and Pierre Fabre. B.P.F. received support with conference travel from BMS.

Additional information

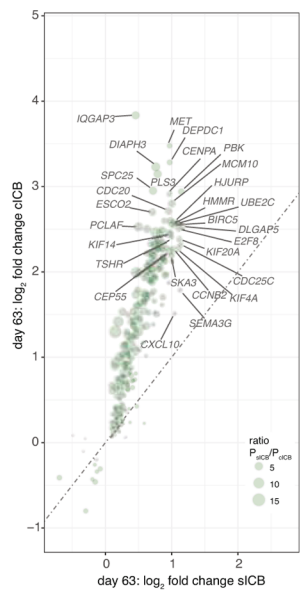
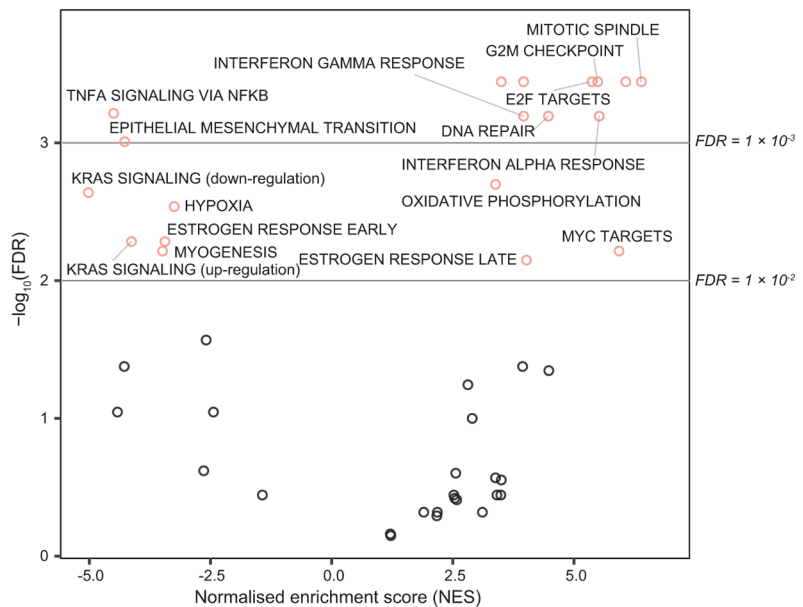
Extended data is available for this paper at <https://doi.org/10.1038/s41591-019-0734-6>.

Supplementary information is available for this paper at <https://doi.org/10.1038/s41591-019-0734-6>.

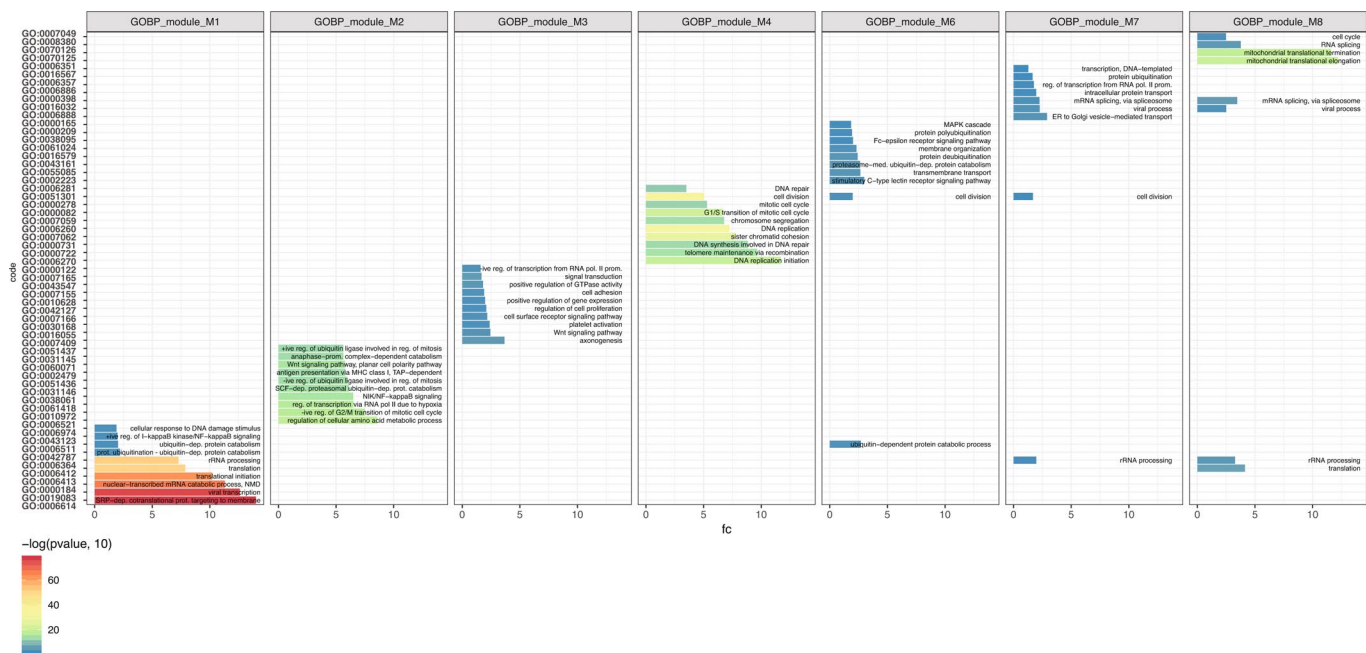
Correspondence and requests for materials should be addressed to B.P.F.

Peer review information Saheli Sadanand was the primary editor on this article and managed its editorial process and peer review in collaboration with the rest of the editorial team.

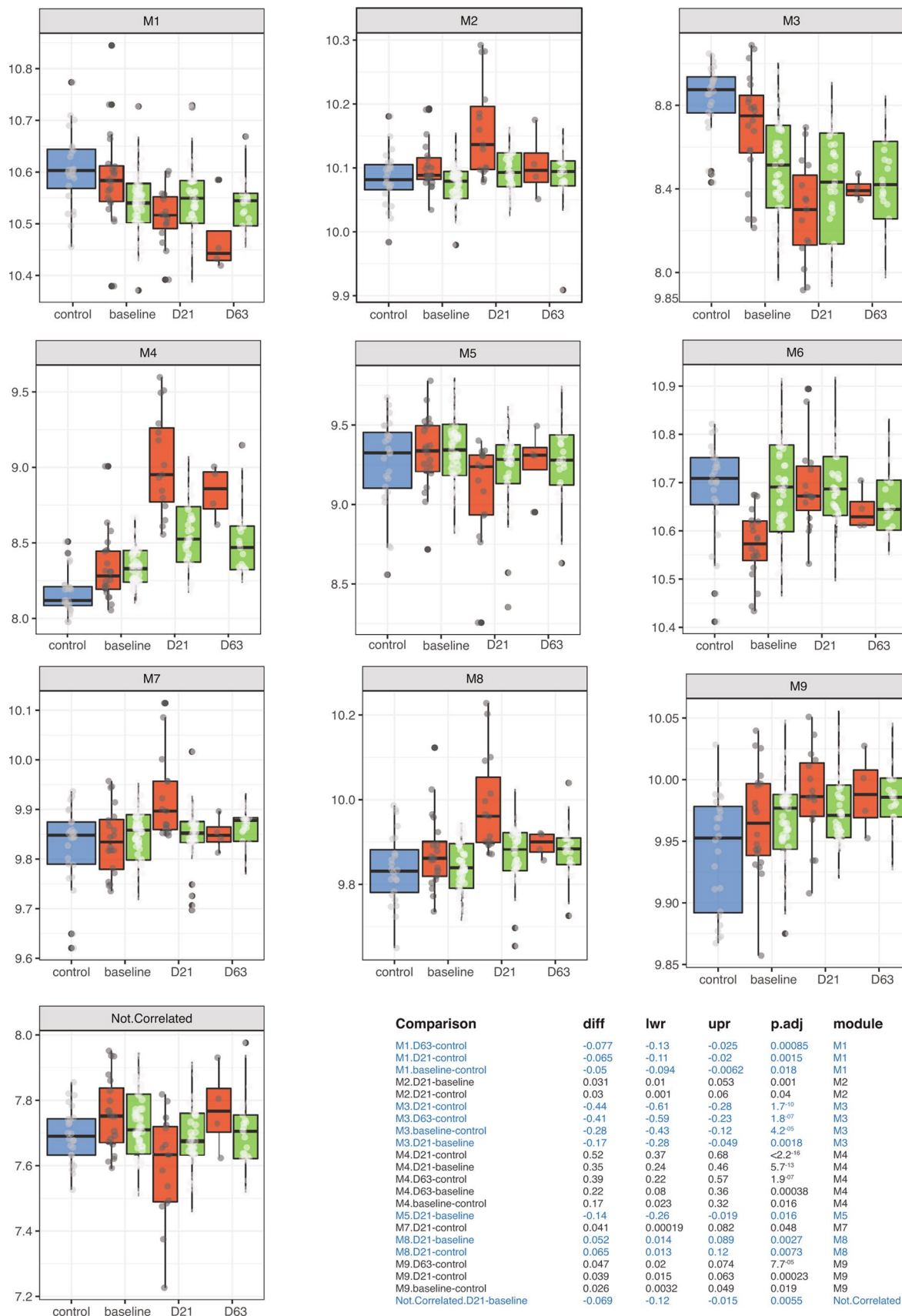
Reprints and permissions information is available at www.nature.com/reprints.

a**b**

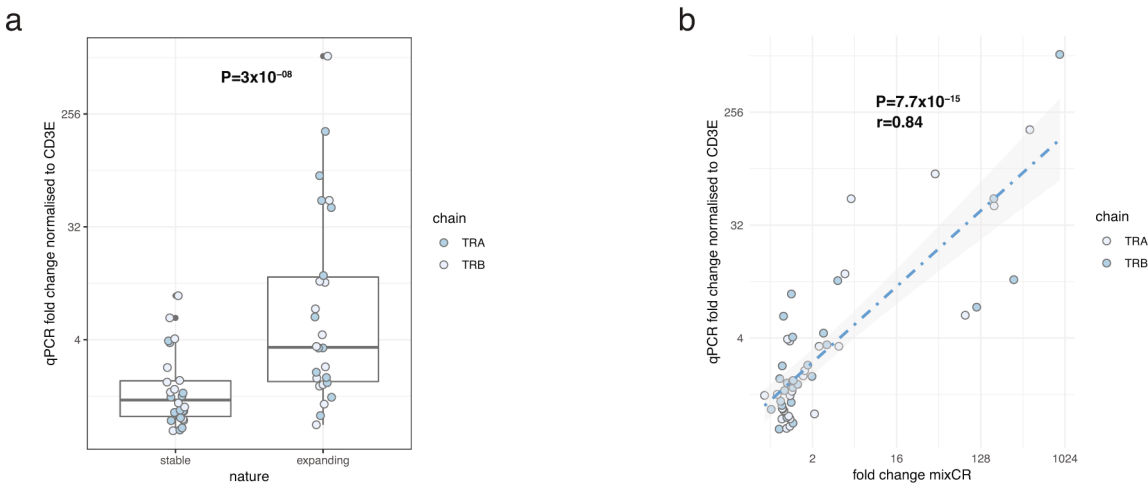
Extended Data Fig. 1 | Extended transcriptomic response to ICB. **a**, Comparison of differential induction of genes by clICB (log fold change y-axis) and sICB (log fold change x-axis) at day 63 (n=46 paired samples, 35 sICB, 11 clICB). **b**, Pathways preferentially upregulated (NES score >0) or suppressed by clICB versus sICB as identified by Gene Set Enrichment analysis depicted in Fig. 1e, f.



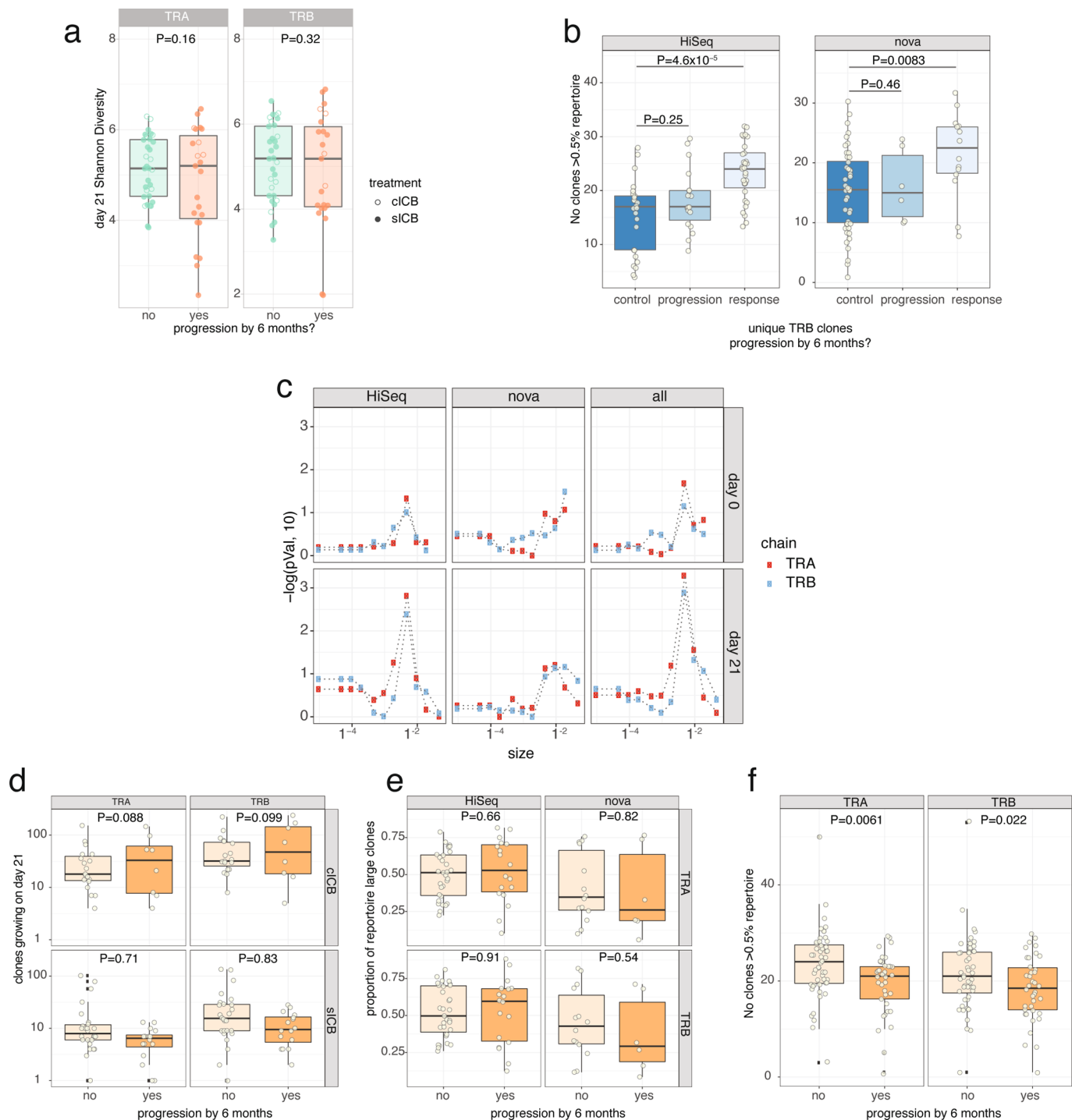
Extended Data Fig. 2 | Module pathways. Pathway analysis was performed using Gene Ontology Biological Processes across treatment response associated modules. For 7/9 modules, transcripts within the modules were significantly associated with discrete processes, with limited overlap between modules. These modules (M1:M4, M6:M8) and all associated pathways for them (FDR <0.05) are listed above. GO specific pathway codes are listed on the y-axis.



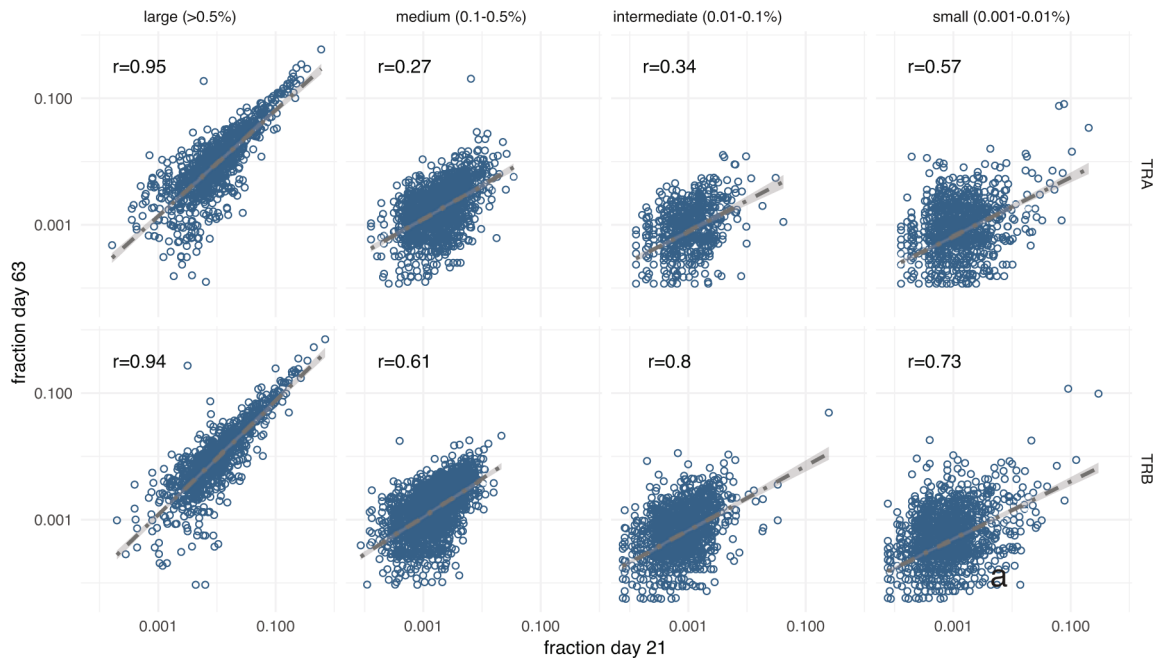
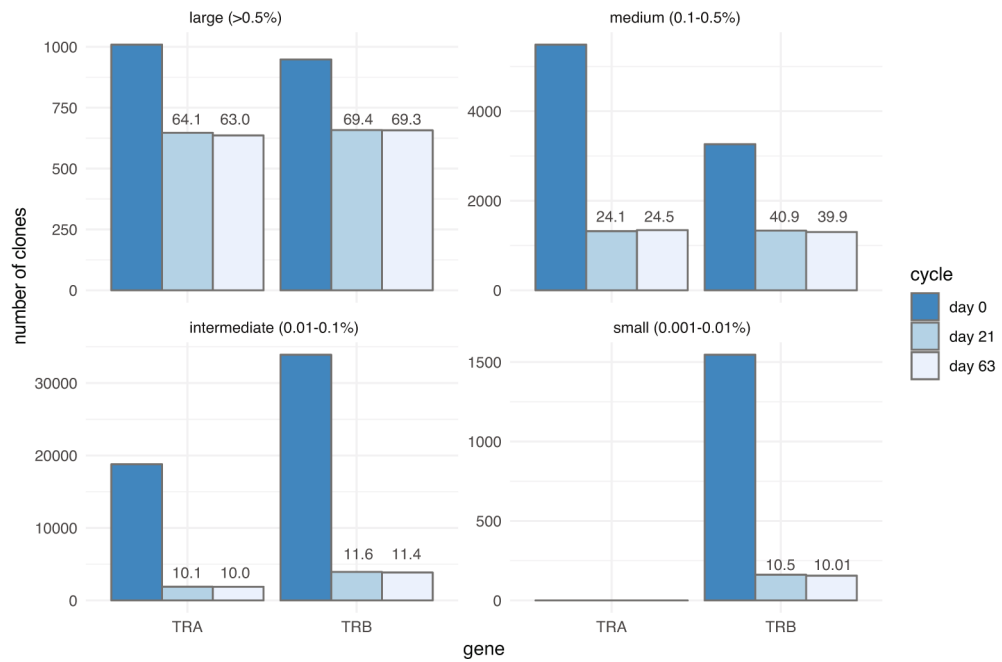
Extended Data Fig. 3 | Module expression. Graphs demonstrate average gene expression per module for each sample with red boxplots and associated points representing clCB samples ($n=20$ baseline, $n=16$ D21, $n=5$ D63) and green boxplots and associated points representing sICB samples ($n=56$ baseline, $n=41$ D21, $n=26$ D63). Controls are untreated healthy volunteers ($n=24$). All statistically significant differences (Tukey adjusted $P < 0.05$) are denoted with associated test in the table and refer to both treatments as group, D21= day 21 sample, D63= day 63 sample.



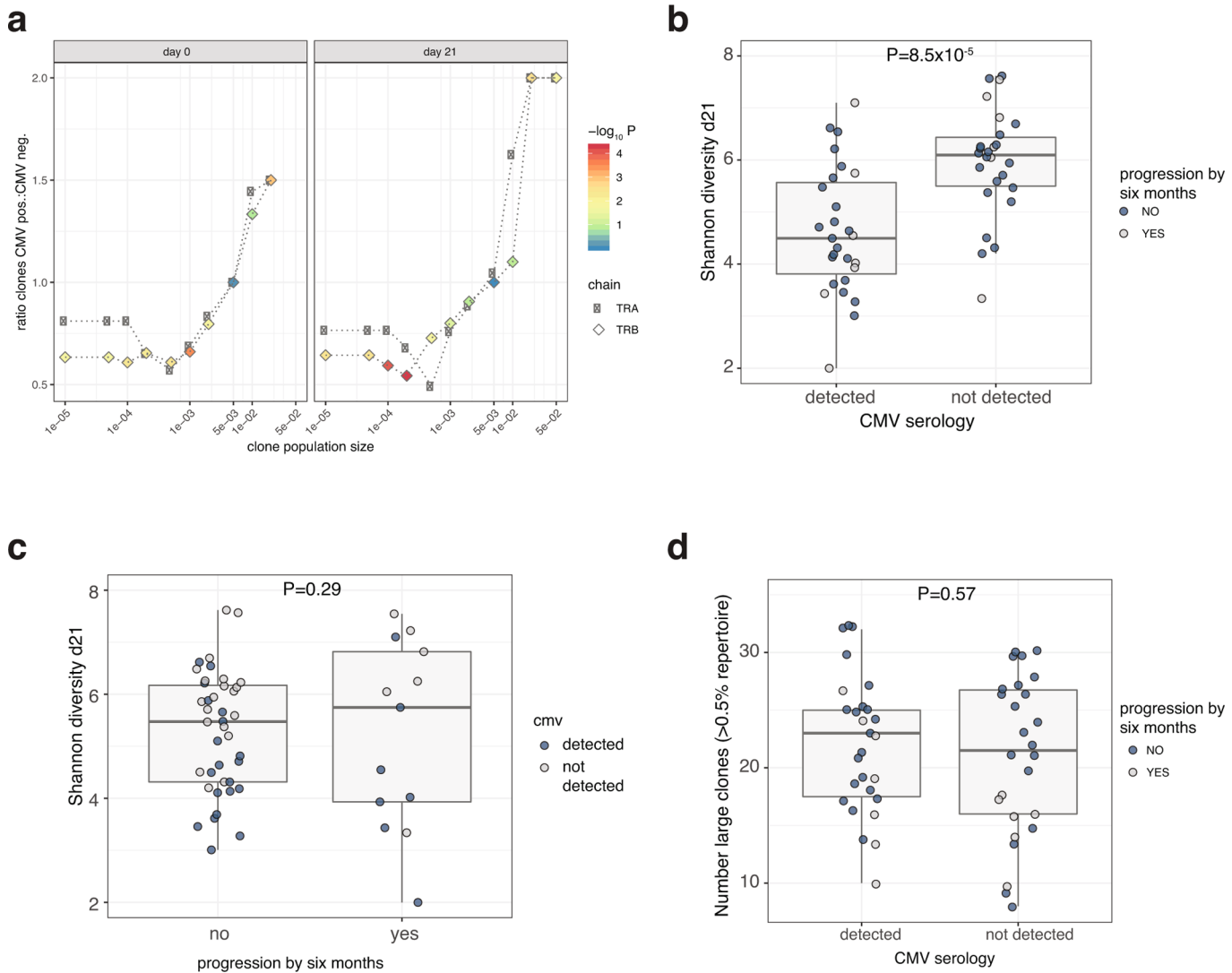
Extended Data Fig. 4 | TCR qPCR. Validation of MiXCR results using quantitative PCR. For n=13 individuals, 2 TCR α and 2 β chains were identified according to whether or not MiXCR reported significant expansion on day 21 versus baseline. Primers were designed to the complementarity determining region 3 (CDR3) sequences for each chain and quantitative PCR performed on pre-treatment day 0 PBMC cDNA and PBMC cDNA from day 21. Ct values were normalized to total expression of CD3E. **a**, Clones identified as expanding in the MiXCR CD8 $^{+}$ RNA were found to show significantly more expansion (median 3.48 fold, IQR 1.85-12.79) than non expanding (median 1.32 fold, IQR 0.97-1.88, Wilcoxon signed-rank Test (two-sided) P=3x10⁻⁸⁸). Lower and upper hinge of box on boxplots represent 25-75th percentiles, central line the median and the whiskers extend to largest and smallest values no greater than 1.5x interquartile range. **b**, MiXCR fold change per clone from CD8 $^{+}$ cells was highly correlated with that determined from bulk PBMCs using quantitative PCR (Pearson correlation, two-sided T-statistic).



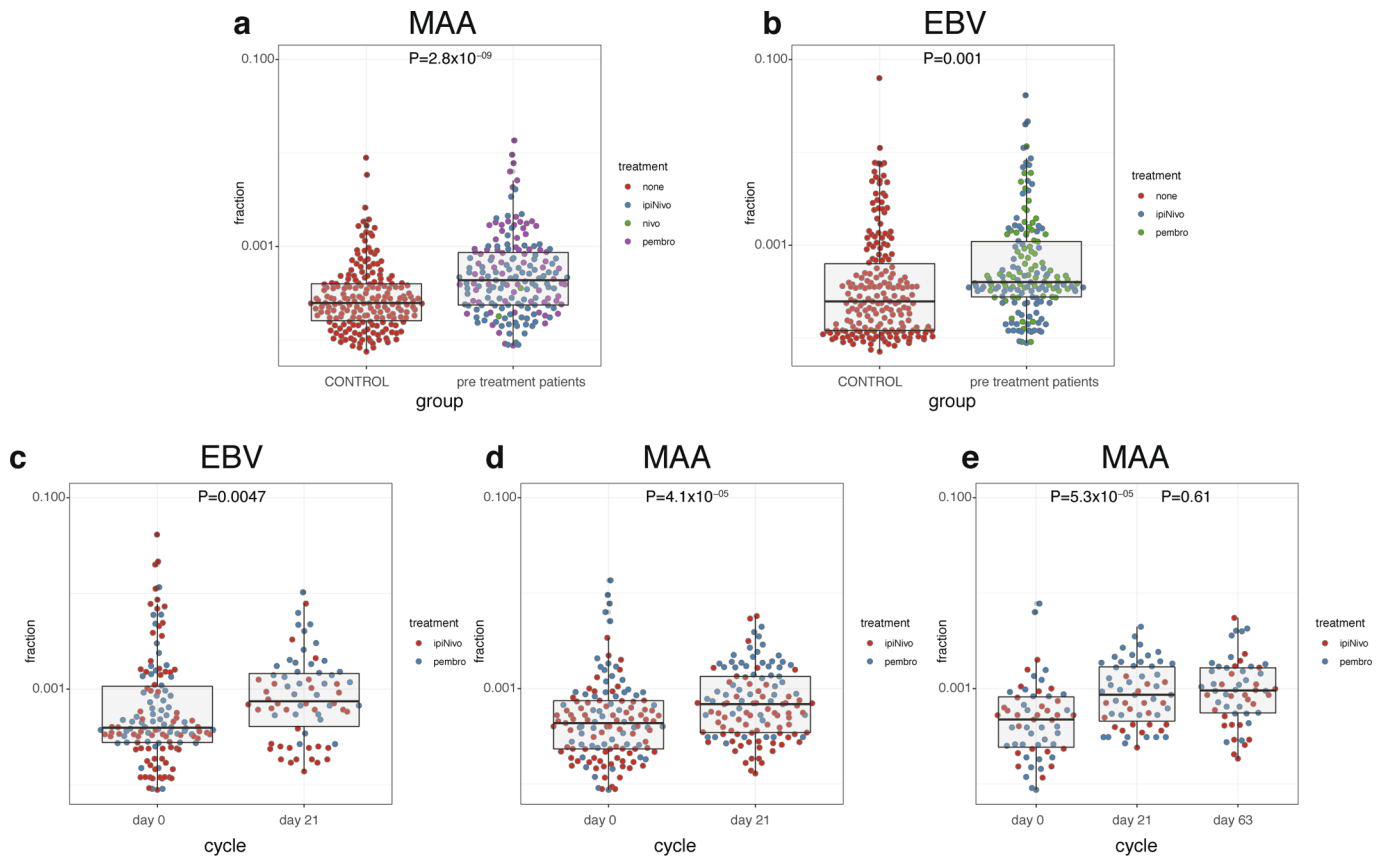
Extended Data Fig. 5 | Extended clone size analysis. **a**, Day 21 post ICB clonal diversity is similar in patients who have 6-month response versus those with disease progression by this timepoint (two-sided T-test, n=69). **b**, As per Fig. 3a, but with unique clones defined by the β -chain, left panel two-sided Wilcoxon signed-rank Test (n=25 controls, 49 patients, right panel one-sided Wilcoxon signed-rank Test, n=43 controls, 20 patients). **c**, Threshold for clone size associating with outcome, x-axis indicates size of clone with test comparing number of clones above that size according to clinical outcome, y-axis: $-\log_{10}(p\text{-value})$ from test. The difference between responding patients and progressing patients being maximal at clone size of 0.5% (two-sided Wilcoxon test, n=69). **d**, Across all samples there is no association between number of clones growing on day 21 ($P<0.05$) and clinical outcome by treatment type. **e**, Proportion of repertoire contributed by large clones does not differ according to clinical outcome. **f**, When all cutaneous patients are grouped a significant association between pre-treatment large clone count and outcome is observed (n=89, Wilcoxon rank-sum, one-sided test). For all boxplots lower and upper hinges of box represent 25–75th percentiles, central line the median and the whiskers extend to largest and smallest values no greater than 1.5x interquartile range.

a**b**

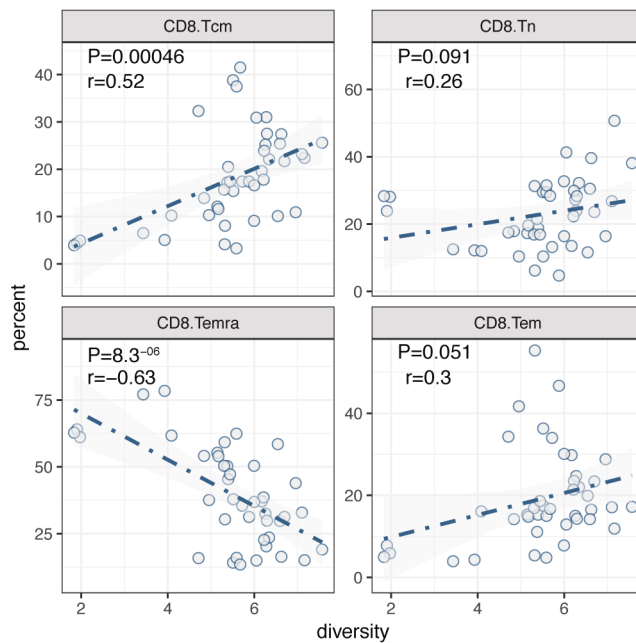
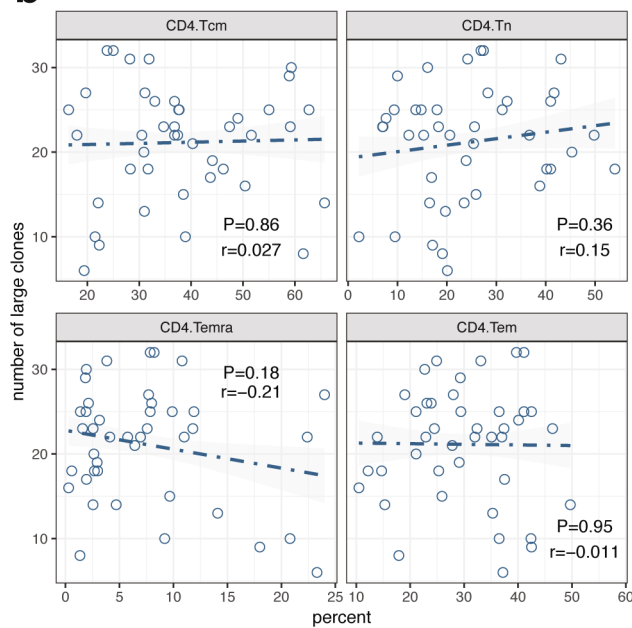
Extended Data Fig. 6 | Temporal stability of clones. **a**, Clones from 42 individuals with samples at 3 timepoints were identified at day 0 pre-treatment and classified according to size. The corresponding correlation for the same clones between day 21 and day 63 was assessed (Pearson correlation, two-sided T-statistic all $P < 2.2 \times 10^{-16}$), demonstrating large clones show greater stability in proportion of clonal space occupied over time. **b**, Clones identified pre-treatment were assessed at day 21 and day 63 with bar plot values representing the number that were larger than the lower defining value of the bin (e.g. $>0.01\%$ for intermediate) at later timepoints, the values on top of bars represent percentage of day 0 recovery.



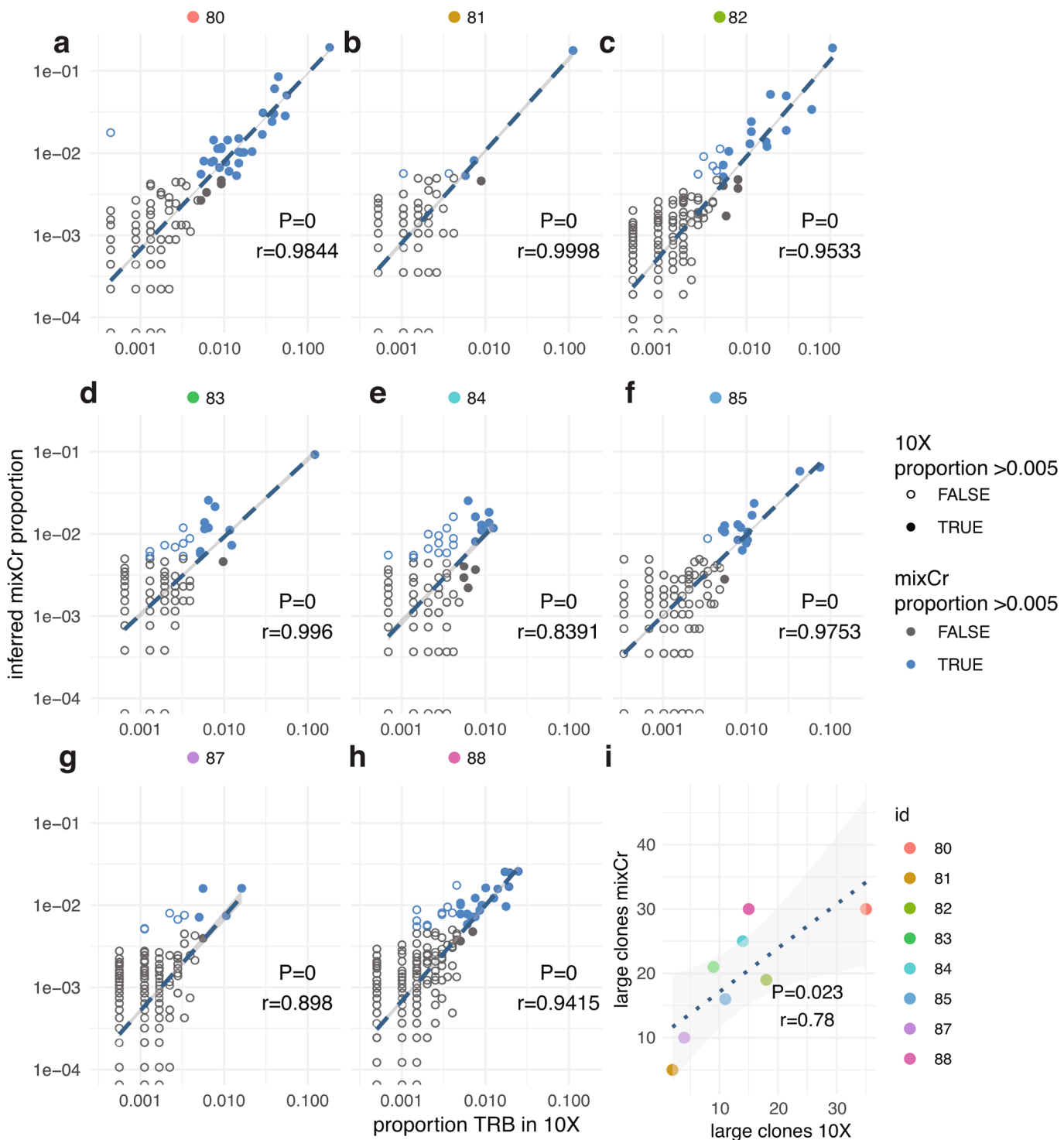
Extended Data Fig. 7 | Effect of CMV. For a subset of cutaneous melanoma patients with day 21 data we were able to measure unequivocal CMV serology. **a**, CMV seropositivity is associated with a depletion of small clones (ratio <1 for clones <0.05% repertoire) and increased numbers of large clones (>2% repertoire) (n=68 left panel, 53 right panel). **b**, Patients seropositive for CMV demonstrated significantly reduced CD8⁺ TCR diversity at day 21 (measured on TRB CDR3) (n=53, two-sided T-Test). **c**, Despite significant differences in diversity from CMV there was no difference in diversity between day 21 samples from progressing and responding patients (n=53, two-sided T-test). **d**, There is no association between CMV serology and number of large clones at day 21 (n=53, two-sided T-Test) For all boxplots lower and upper hinges of box represent 25–75th percentiles, central line the median and the whiskers extend to largest and smallest values no greater than 1.5x interquartile range.



Extended Data Fig. 8 | Comparison of clonotypes to public clones. **a**, The complete dataset of clones were screened for public clonotypes for melanoma associated-antigens (MAA), demonstrating that the size of clones matching these clonotypes in untreated melanoma patients is significantly greater than those in controls (Wilcoxon Test, $n=106$ patients, 68 controls). **b**, Melanoma patients showed no difference in mean EBV reactive clone size from controls ($P>0.05$) although the distribution of clones was skewed in non-melanoma patients and median clone size greater in patients (two-way Wilcoxon-Test). **c**, Treatment led to a small increase in median EBV reactive clonotype clone size across all patients, but **d**, the significance of this effect was greater for MAA clonotypes **e**, for samples with data for clone sizes at day 63 as well as day 21 ($n=41$ individuals) there was no further change in clone size at the later timepoint (two-way Wilcoxon-Test). For all boxplots lower and upper hinges of box represent 25–75th percentiles, central line the median and the whiskers extend to largest and smallest values no greater than 1.5x interquartile range.

a**b**

Extended Data Fig. 9 | Investigating flow correlates of clonal indices. **a**, For 42 samples from 19 patients, blinded flow cytometry data to assess CD8⁺ subsets (Tcm: central memory, Tn: naive, Temra: effector memory re-expressing CD45RA, Tem: effector memory) was integrated with the Shannon diversity index calculated for each sample. This demonstrated a strong positive association between TCM and diversity, whereas TEMRA was significantly anticorrelated with diversity (Pearson correlation, two way T-statistic). **b**, as per Fig. 3e, except here large clone count was correlated with percentage CD4⁺ subsets from each of the samples. Unlike for CD8⁺ cells, there is no association between large clone count and percentage CD4⁺ subset in the samples analysed (Pearson correlation, two way T-statistic).



Extended Data Fig. 10 | Comparing MiXCR and 10X TCR data. **a–h**, For 8 patients, indicated by number, CD8⁺ cell samples were subject to 10X chromium single cell 5' RNA sequencing providing T cell receptor sequencing and standard bulk sequencing (see methods). Clones were identified by their β chain and for each productive β chain identified the relative clonal proportion (frequency) was calculated. Clones were matched via the CDR3 amino acid sequence with β chains from the same samples mapped from bulk CD8⁺ cell RNA using MiXCR. Where the clone fell below detection limit in MiXCR a value of 0 was attributed. MiXCR clones were identified for 92.1% clones >0.1% population in 10X (6990/7597) and 99.4% clones >0.2% size (5816/5852). x-axis=10X proportion, y-axis MiXCR proportion, r calculated using Pearson correlation coefficient, all $P<2.2\times 10^{-16}$. **i**, Despite the different methods, the number of large clones (>0.5% total clonal population) identified from 10X and MiXCR approaches are correlated.

Corresponding author(s): Benjamin Fairfax

Last updated by author(s): Nov 5, 2019

Reporting Summary

Nature Research wishes to improve the reproducibility of the work that we publish. This form provides structure for consistency and transparency in reporting. For further information on Nature Research policies, see [Authors & Referees](#) and the [Editorial Policy Checklist](#).

Statistics

For all statistical analyses, confirm that the following items are present in the figure legend, table legend, main text, or Methods section.

n/a Confirmed

- The exact sample size (n) for each experimental group/condition, given as a discrete number and unit of measurement
- A statement on whether measurements were taken from distinct samples or whether the same sample was measured repeatedly
- The statistical test(s) used AND whether they are one- or two-sided
Only common tests should be described solely by name; describe more complex techniques in the Methods section.
- A description of all covariates tested
- A description of any assumptions or corrections, such as tests of normality and adjustment for multiple comparisons
- A full description of the statistical parameters including central tendency (e.g. means) or other basic estimates (e.g. regression coefficient) AND variation (e.g. standard deviation) or associated estimates of uncertainty (e.g. confidence intervals)
- For null hypothesis testing, the test statistic (e.g. F , t , r) with confidence intervals, effect sizes, degrees of freedom and P value noted
Give P values as exact values whenever suitable.
- For Bayesian analysis, information on the choice of priors and Markov chain Monte Carlo settings
- For hierarchical and complex designs, identification of the appropriate level for tests and full reporting of outcomes
- Estimates of effect sizes (e.g. Cohen's d , Pearson's r), indicating how they were calculated

Our web collection on [statistics for biologists](#) contains articles on many of the points above.

Software and code

Policy information about [availability of computer code](#)

Data collection

Flow cytometry data was collected using FlowJo version 10

Data analysis

R version 3.4.3, R packages: Deseq2 (1.18.1), ggplot2(3.0.0), vegan(2.5-1), CEMiTool (1.0.3), XGR (1.1.5), Seurat (3.02). RNA sequences were mapped with HISAT (2.1.0) and counts retrieved with HTseq-count (0.5.4p5). Single cell sequencing mapped with Cell ranger(3.1.0). TCR were mapped using MiXCR (v3.0.10). All variables are listed in the methods.

For manuscripts utilizing custom algorithms or software that are central to the research but not yet described in published literature, software must be made available to editors/reviewers. We strongly encourage code deposition in a community repository (e.g. GitHub). See the Nature Research [guidelines for submitting code & software](#) for further information.

Data

Policy information about [availability of data](#)

All manuscripts must include a [data availability statement](#). This statement should provide the following information, where applicable:

- Accession codes, unique identifiers, or web links for publicly available datasets
- A list of figures that have associated raw data
- A description of any restrictions on data availability

Data Availability: All sequencing data will be made freely available to organisations and researchers to conduct research in accordance with the UK Policy Framework for Health and Social Care Research via a Data Access Agreement. Sequence data has been deposited at the European Genome-phenome Archive (EGA), which is hosted by the EBI and the CRG, under accession number EGAS00001004081. Patient anonymized raw flow cytometry data will be promptly made freely accessible for download from the MRC WIMM server on application.

Field-specific reporting

Please select the one below that is the best fit for your research. If you are not sure, read the appropriate sections before making your selection.

- Life sciences Behavioural & social sciences Ecological, evolutionary & environmental sciences

For a reference copy of the document with all sections, see nature.com/documents/nr-reporting-summary-flat.pdf

Life sciences study design

All studies must disclose on these points even when the disclosure is negative.

Sample size	Empirical analysis of RNA sequencing data demonstrated paired cohorts of 10+ provide power to detect ICB associated gene expression changes after multiple comparison testing. Sample size was determined by number of available patients who met clinical inclusion criteria (e.g. metastatic melanoma treated with single agent anti-PD1 or combination anti-CTLA4/anti-PD1 therapy) who had provided informed consent and had CD8 T-cell RNA samples available.
Data exclusions	Response rates to checkpoint immunotherapy are lower in uveal and mucosal melanoma versus cutaneous melanoma and only samples from patients with a clinical history of definite or most likely cutaneous melanoma were included in the analysis of clinical outcomes. This is stated in the main body of the text and the methods. Supplementary Table 1 lists all samples for the analysis and exclusions from different aspects are detailed if and where appropriate - 4 sequencing files showing potential sample contamination (>2.5%) were excluded from outcome analysis. Similarly, 1 individual was excluded from outcome analysis due to equivocal metastases on radiology.
Replication	The difference between control samples and responding melanoma patients in terms of the number of large T-cell clones was replicated in a second set of individuals from the Oxford Biobank and healthy controls who were processed at a later timepoint.
Randomization	All covariates used are listed in the methods. The main comparisons within the dataset are treated versus untreated patient samples, and samples from patients who demonstrate disease progression at the 6 month timepoint, versus those who do not. Thus, this analysis was not amenable to randomization.
Blinding	For flow cytometry analysis the investigator (C.A.T.) was blinded to all clinical and bioinformatic data from patients. There were no other experiments amenable to blinding.

Reporting for specific materials, systems and methods

We require information from authors about some types of materials, experimental systems and methods used in many studies. Here, indicate whether each material, system or method listed is relevant to your study. If you are not sure if a list item applies to your research, read the appropriate section before selecting a response.

Materials & experimental systems		Methods	
n/a	Involved in the study	n/a	Involved in the study
<input type="checkbox"/>	<input checked="" type="checkbox"/> Antibodies	<input checked="" type="checkbox"/>	<input type="checkbox"/> ChIP-seq
<input checked="" type="checkbox"/>	<input type="checkbox"/> Eukaryotic cell lines	<input type="checkbox"/>	<input checked="" type="checkbox"/> Flow cytometry
<input checked="" type="checkbox"/>	<input type="checkbox"/> Palaeontology	<input checked="" type="checkbox"/>	<input type="checkbox"/> MRI-based neuroimaging
<input checked="" type="checkbox"/>	<input type="checkbox"/> Animals and other organisms		
<input type="checkbox"/>	<input checked="" type="checkbox"/> Human research participants		
<input type="checkbox"/>	<input checked="" type="checkbox"/> Clinical data		

Antibodies

Antibodies used	Antibody Clone Conjugate Supplier LIVE/DEAD™ Fixable Near-IR Dead Cell Stain Kit ThermoFisher Scientific Mouse anti-human CD3 UCHT1 BV785 BioLegend, Lot: B254354, 1:25 dilution Mouse anti-human CD56 5.1H11 BV421 BioLegend, Lot:B265662, 1:50 dilution Mouse anti-human CD4 RPA-T4 APC BioLegend, Lot: B267987, 1:50 dilution Mouse anti-human CD8alpha RPA-T8 BV510 BioLegend, Lot:B272192, 1:25 dilution Mouse anti-human CD45RA HI100 FITC Becton Dickinson, Lot: 8037739, 1:50 dilution Mouse anti-human CD27 M-T271 AF700 BioLegend, Lot: B245610, 1:50 dilution
Validation	As per manufacturers. Bead controls used for flow.

Human research participants

Policy information about [studies involving human research participants](#)

Population characteristics	Control samples were collected via the Oxford biobank (www.oxfordbiobank.org.uk) with full ethical approval (REC 06/Q1605/55) and written informed consent from healthy volunteers of European ancestry between the ages of 24–61 (median age 49.5, IQR 34–54).
Recruitment	They had previously enrolled within the Oxford Biobank prior to conception of this study.
Ethics oversight	Local ethical approval REC 06/Q1605/55 for healthy control samples, Oxford Radcliffe Biobank (South Central Oxford C REC: 09/H0606/5+5) for samples in the Oxford Radcliffe Biobank (clinical samples).

Note that full information on the approval of the study protocol must also be provided in the manuscript.

Clinical data

Policy information about [clinical studies](#)

All manuscripts should comply with the ICMJE [guidelines for publication of clinical research](#) and a completed [CONSORT checklist](#) must be included with all submissions.

Clinical trial registration	The study is an observational study with patients donating samples to the Oxford Radcliffe Biobank (South Central Oxford C REC: 09/H0606/5+5) upon initiation of care for melanoma.
Study protocol	All methods are recorded in the paper
Data collection	Samples were collected from patients at onset of immunotherapy (i.e. blood taken upon cannulation for treatment). Subsequent samples were taken after sequential cycles of treatment as listed (with day 21 samples corresponding to those taken immediately prior to the second cycle of immunotherapy).
Outcomes	All samples were obtained from patients receiving standard of care treatment within the NHS and outcomes were defined clinically or using radiological assessment according to irRECIST.1.1 performed approximately 12 & 24 weeks post-initiation of treatment. Progressors were defined as those with radiographic disease progression at either of these two-time points or who had unequivocal rapid disease progression necessitating cessation of ICB treatment. Outcomes were dichotomised according to evidence of radiological disease stability or response for the minimum duration of 24 weeks .

Flow Cytometry

Plots

Confirm that:

- The axis labels state the marker and fluorochrome used (e.g. CD4-FITC).
- The axis scales are clearly visible. Include numbers along axes only for bottom left plot of group (a 'group' is an analysis of identical markers).
- All plots are contour plots with outliers or pseudocolor plots.
- A numerical value for number of cells or percentage (with statistics) is provided.

Methodology

Sample preparation	PBMCs were prepared, frozen and stored in liquid Nitrogen in 90%FBS/10% DMSO for later use in flow. Samples were thawed and staining antibodies and dye clones, dilutions and manufacturer shown in Extended figure 12. Cells were stained in HBSS containing 5% fetal calf serum on ice and in the dark for 30 minutes, then fixed in 2% paraformaldehyde. All samples included fixable amine reactive viability dye.
Instrument	LSR II
Software	FlowJo version 10
Cell population abundance	N/A
Gating strategy	Supplementary Figure 2

- Tick this box to confirm that a figure exemplifying the gating strategy is provided in the Supplementary Information.